On the Predominant Nonlinear Response of the Extratropical Atmosphere to Meridional Shifts of the Gulf Stream

HYODAE SEO, YOUNG-OH KWON, TERRENCE M. JOYCE, AND CAROLINE C. UMMENHOFER

Physical Oceanography Department, Woods Hole Oceanographic Institution, Woods Hole, Massachusetts

(Manuscript received 29 September 2016, in final form 6 September 2017)

ABSTRACT

The North Atlantic atmospheric circulation response to the meridional shifts of the Gulf Stream (GS) path is examined using a large ensemble of high-resolution hemispheric-scale Weather Research and Forecasting Model simulations. The model is forced with a broad range of wintertime sea surface temperature (SST) anomalies derived from a lag regression on a GS index. The primary result of the model experiments, supported in part by an independent analysis of a reanalysis dataset, is that the large-scale quasi-steady North Atlantic circulation response is remarkably nonlinear about the sign and amplitude of the SST anomaly chosen over a wide range of GS shift scenarios. The nonlinear response prevails over the weak linear response and resembles the negative North Atlantic Oscillation (NAO), the leading intrinsic mode of variability in the model and the observations. Further analysis of the associated dynamics reveals that the nonlinear responses are accompanied by the shift of the North Atlantic eddy-driven jet, which is reinforced, with nearly equal importance, by the high-frequency transient eddy feedback and the low-frequency wave-breaking events. Additional sensitivity simulations confirm that the nonlinearity of the circulation response is a robust feature found over the broad parameter space encompassing not only the varied SST but also the absence/presence of tropical influence, the varying lateral boundary conditions, and the initialization scheme. The result highlights the fundamental importance of the intrinsically nonlinear transient eddy dynamics and the eddy–mean flow interactions in generating the nonlinear downstream response to the meridional shifts in the Gulf Stream.

1. Introduction

Air–sea interaction over the western boundary currents is one of the fundamental processes of extratropical climate variability (Kwon et al. 2010; Kelly et al. 2010). In the North Atlantic, the largest surface heat flux and its strongest interannual variability are found over the Gulf Stream (GS). The variations in the location and strength of the GS modify the cyclogenesis and the North Atlantic storm track (Cione et al. 1993; Booth et al. 2012; Small et al. 2014), potentially influencing the broader-scale atmospheric and climate variability (Minobe et al. 2008; O'Reilly et al. 2016, 2017).

Because of the potential basin-scale importance, the position of the GS path has been monitored for many decades (Rossby and Gottlieb 1998; Kelly et al. 1999; Taylor and Stephens 1998). To evaluate the GS influence on the large-scale circulation, this study adopts the subsurface temperature-based proxy for the GS position defined by Joyce et al. (2000). The GS index (GSI) is defined as the leading empirical orthogonal function (EOF) mode, explaining >50% of the total variance, of the meridional shift at 9 locations of the 15°C isotherm at 200-m depth over 75°–55°W. The GSI is available for 1954–2013 at a seasonal resolution. The winter (January–March) GSI, detrended and normalized to unit standard deviation, is shown in Fig. 1a, where the positive GSI indicates the northward shift. The winter GS position is known to exhibit substantial interannual to decadal variations in association with the North Atlantic Oscillation (NAO) (Taylor and Stephens 1998; Joyce et al. 2000; Frankignoul et al. 2001). The GS is displaced northward (southward) when the NAO is in the positive (negative) phase, with the NAO leading the GS shift by 12–18 months (Frankignoul et al. 2001; Sanchez-Franks et al. 2016). The lag is explained by the adjustment time scale of the GS position to the NAO-driven wind stress and wind stress curl (Gangopadhyay et al. 1992). However, Frankignoul et al. (2001) found no evidence that the GS SST anomaly exerts a direct impact

Corresponding author: Hyodae Seo, hseo@whoi.edu

DOI: 10.1175/JCLI-D-16-0707.1

© 2017 American Meteorological Society. For information regarding reuse of this content and general copyright information, consult the AMS Copyright Policy (www.ametsoc.org/PUBSReuseLicenses).

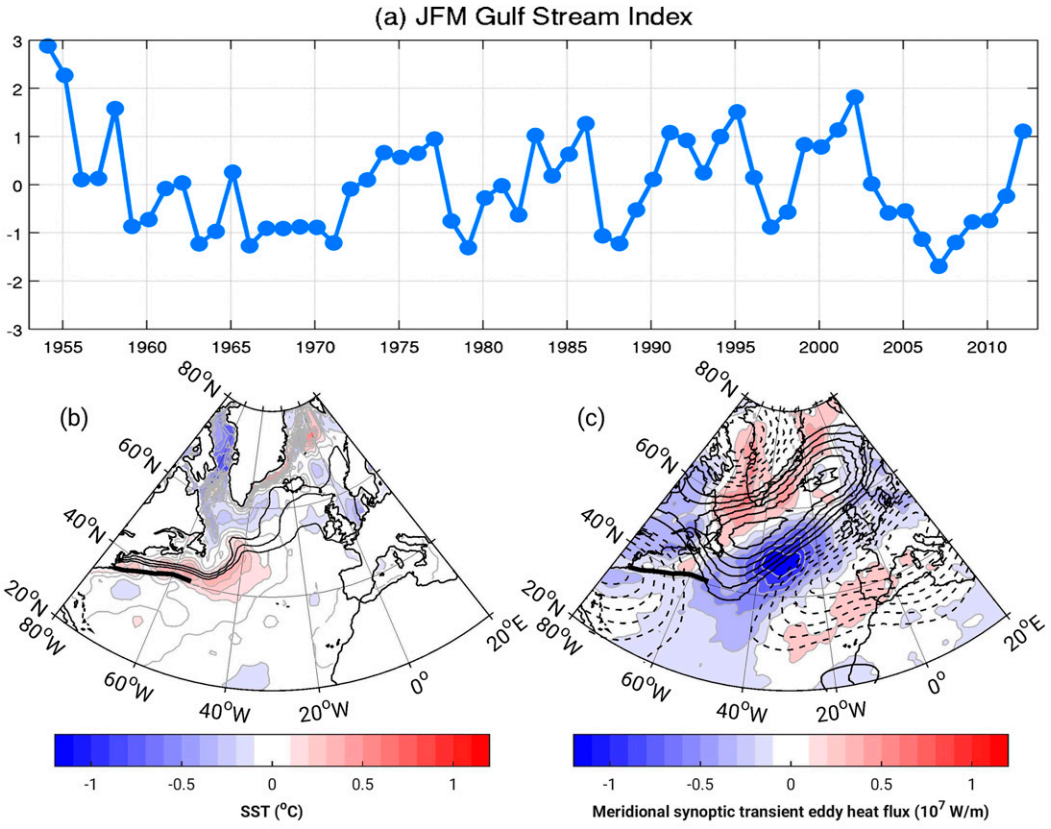

FIG. 1. (a) Detrended and normalized (to unit standard deviation) JFM GSI (Joyce et al. 2000) for the period 1954–2012. (bottom) The linearly regressed (b) SST (color shading, °C) and (c) column-integrated (1000–50 hPa) northward synoptic eddy heat flux (color shading, 10^7 W m^{-1}) overlaid with the Z_{250} (m, CI = 2) when the JFM GSI leads by 1 yr (Kwon and Joyce 2013). In (b) and (c), the mean position of the GS is shown as thick black lines; and in (b) the 6°, 8°, and 10°C isotherms by thin black contours. Tropical influence is removed based on the linear regression on the leading principal components of the tropical Indo-Pacific SST and tropical Atlantic SST.

on the large-scale circulation. In contrast, Wills et al. (2016) identified the significant transient atmospheric circulation responses that lag the SST anomalies in the GS extension by several weeks, with the pattern of response characterized by the anomalous low (high) sea level pressure (SLP) over the GS region (south of Iceland). Similarly, O'Reilly et al. (2017) found the northward shift of the North Atlantic eddy-driven jet and the increase in European blocking frequency in response to the GS SST front (see also O'Reilly et al. 2016).

Focusing on interannual to longer time scales, Kwon and Joyce (2013) used lead–lag regression analysis to find a significant relationship between the GSI and the North Atlantic SST when the GSI leads by 1 yr in the absence of the tropical influence. The corresponding regressed SST pattern is shown in Fig. 1b. For the GS displaced northward by a unit standard deviation (normalized σ), a warm SST anomaly up to 0.4°C emerges from Cape Hatteras toward the Grand Banks and downstream of the GS. The SST anomaly of the opposite sign and weaker amplitude (~0.2°C) is found to the north, representing the strength of the subpolar gyre. Since the observed range of the GSI remains within $\pm 3\sigma$ (Fig. 1a), the amplitude of the corresponding SST anomaly is expected to be within ±1°C. In response to the SST anomaly, the significant reduction in the transient eddy heat flux (shading), accompanied by the enhanced 250-hPa geopotential height Z_{250} that is in quadrature (contours), can be detected downstream of the GS toward Scandinavia and the Nordic Sea (Fig. 1c). The enhanced transient eddy activity and anomalous troughs are also found near Greenland and over western Europe. The eddy flux and the Z_{250} patterns overall suggest an NAO-like response in the atmospheric circulation to the GS SST anomaly.

Using atmospheric general circulation models (AGCMs), a number of studies demonstrated the North Atlantic SST anomaly influences not only the storm track (e.g., Kushnir et al. 2002; Palmer and Sun 1985, Peng et al. 1995; Woollings et al. 2010a; Small et al. 2014;

Piazza et al. 2016) but also the low-frequency atmospheric circulation far downstream (Peings and Magnusdottir 2014; O'Reilly et al. 2016). The diabatic forcing associated with an SST anomaly initiates a baroclinic adjustment in the atmosphere near the forcing region (Hoskins and Karoly 1981; Li and Conil 2003; Ferreira and Frankignoul 2005), which is linear about the sign and size of the SST anomaly (Deser et al. 2007). However, the overall large-scale response has an equivalent barotropic structure with no strong resemblance to the prescribed SST anomaly pattern (Ferreira and Frankignoul 2005, 2008; Kushnir and Lau 1992; Robinson 2000; Seo et al. 2014). The transformation from the linear to the quasi-steady nonlinear response is facilitated by the two energetic circulation adjustment processes. On one hand, the transient eddy feedback reinforces the formation of the blocking ridge in the high-latitude North Atlantic via anomalous vorticity flux convergence (Shutts 1983; Haines and Marshall 1987; Lau and Nath 1990; Nakamura and Wallace 1990). On the other hand, the low-frequency dynamics involving the high-latitude wave-breaking and wave-blocking events (Strong and Magnusdottir 2008) influence the position of the North Atlantic eddy-driven jet and the NAO (Rivière and Orlanski 2007; Woollings et al. 2010b). The basin-scale quasi-steady circulation response to extratropical SST forcing often resembles the leading mode of the internal atmospheric variability (Peng and Robinson 2001; Deser et al. 2004; Frankignoul and Sennéchael 2007).

The extratropical SST anomaly used in most AGCM studies, however, is not directly attributed to the shift in GS but instead often reflects the basin-scale modes of variability. Furthermore, the size and scale of the SST anomaly are too large and broad, respectively (e.g., 7°C in Deser et al. 2004). More recent GS-centric studies spatially smooth the GS SST front (Minobe et al. 2008; Kuwano-Yoshida et al. 2010; Small et al. 2014; O'Reilly et al. 2016; Piazza et al. 2016), but the resulting SST anomalies are also too large (e.g., ±6°C is used in Small et al. 2014) compared to the observed range of ±1°C inferred from Fig. 1. Thus, a high-resolution model simulation forced with realistic amplitude and distribution of the SST anomaly is needed to evaluate the relevant dynamical adjustment processes that can be unambiguously attributed to the GS shift. The challenge is to detect a statistically significant response with amplitudes substantially smaller than the level of internal variability in the winter atmosphere.

The goal of this study is to examine the large-scale atmospheric response to lateral displacements of the GS path in the North Atlantic using a large ensemble of simulations and a reanalysis dataset. A wide range of GS shift scenarios with varied combinations of initial and lateral boundary conditions is considered, with some being in the observed range and others representing an unprecedented case. Particular attention will be paid to the dynamical adjustment processes generated by the GS SST anomaly in the model and how these processes influence the steady-state response.

The paper is organized as follows. Section 2 describes the model, experiments, and methods of analysis. Section 3 discusses the modeled internal variability, the time-mean and transient modeled response, the response in precipitation, and the change in background state associated with the shift in the eddy-driven jet. Section 4 focuses on two atmospheric adjustment processes shaping the quasi-stationary response. Section 5 evaluates the influence of initial and lateral boundary conditions. Section 6 looks for evidence of the nonlinear circulation response from a reanalysis dataset. Section 7 is a summary and a discussion.

2. Model, data, and analysis

a. Model

This study uses the Weather Research and Forecasting (WRF) Model (Skamarock et al. 2008), with the domain covering most of the Northern Hemisphere on a polar stereographic projection at 40-km resolution (Fig. 2a). There are 28 terrain-following sigma levels between the surface and 50 hPa, with 10 layers below 750-m height. Cumulus convection is parameterized with the Kain–Fritsch convection scheme (Kain 2004) and the cloud microphysical process by the single-moment 3-class scheme (Hong et al. 2004). WRF is also run with the Rapid Radiative Transfer Model (Mlawer et al. 1997) and the Goddard scheme (Chou and Suarez 1999) for longwave and shortwave radiation transfer. The Noah land surface model is used for the land surface processes (Chen and Dudhia 2001), and the planetary boundary layer is treated with the Yonsei University scheme (Hong et al. 2006) with the Eta surface layer scheme.

b. Experiments

In the control simulation (CTL), WRF is forced with the daily SST climatology (1982–2014) from the ¼° NOAA Optimum Interpolation SST dataset (Reynolds et al. 2007). The initial and lateral boundary conditions are from the 6-hourly climatology (1970–2009), which is estimated from the National Centers for Environmental Prediction (NCEP)–National Center for Atmospheric Research (NCAR) reanalysis 1 (NCEP-1; Kalnay et al. 1996). NCEP-1 is used in this study because of its extended period of availability, which encompasses the

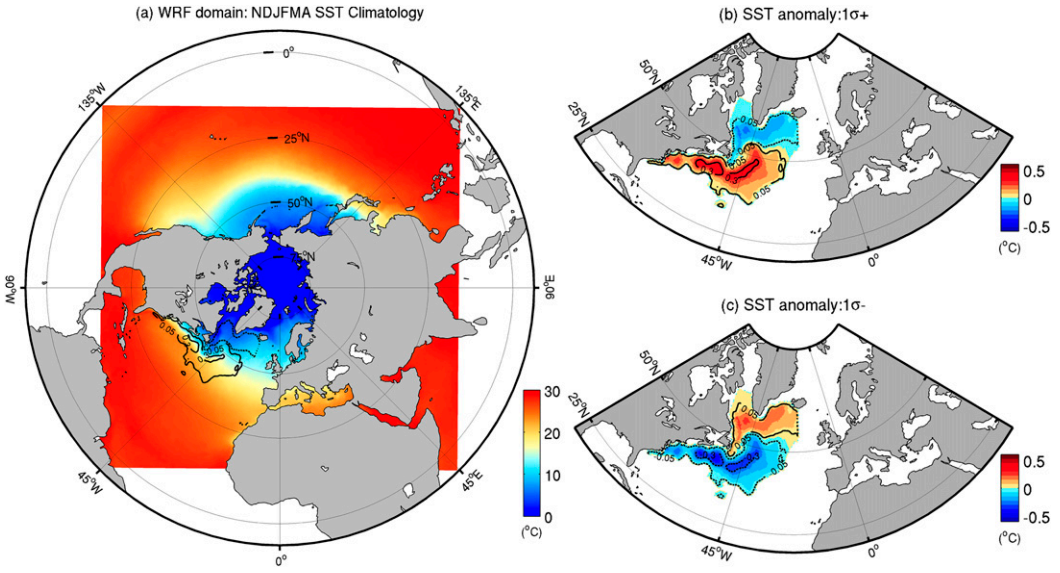

FIG. 2. (a) WRF domain covering the Northern Hemisphere on a polar stereographic projection at 40-km resolution. November–April mean SST climatology (1982–2014, °C, color shading) from the NOAA OI SST dataset. (b) Positive and (c) negative SST anomaly pattern (°C, color shading) when the GS shifts by $1\sigma+$ and $1\sigma-$, respectively.

composite analysis based on the GS index that starts from 1954. Note that using the climatological condition eliminates the remote influence from the deep tropics such as El Niño, so the identified response results only from the extratropical circulation adjustment. However, the sensitivity of the result to the tropical influence is also considered in section 5.

First, 10 sets of SST perturbation simulations are undertaken, which differ from the CTL only in the SST condition in the GS region. Given that the GSI is less than $|\pm 3\sigma|$, the SST anomalies are varied in size from $(1/9)\sigma$ to $(1/3)\sigma$, 1σ, and 3σ (Table 1). An unprecedented case is also considered by using the 9σ SST anomaly. The experiments are repeated with the sign-reversed SST anomaly to examine the linearity and nonlinearity of the response. Each experiment is 6 months long from November to April (NDJFMA), covering the extended Northern Hemisphere winter season. Because of the high internal variability in the winter atmosphere, a robust detection of the forced response to a small SST anomaly requires a large ensemble size. In the present study, each experiment is repeated 40 times with initial conditions that are slightly perturbed with a normally distributed random noise. In section 5, the results from additional experiments with an alternative initialization scheme and varying lateral boundary conditions with the enhanced ensemble size will be presented, where the ensemble initial conditions were sampled from 1 November of each year between 1950 and 2009. The model produces 6-hourly outputs, but the analysis is based on daily averaged quantities. The spatial patterns of SST anomaly for $1\sigma+$ and $1\sigma-$ are shown in Figs. 2b,c. Although each SST anomaly contains both the positive and negative quantities, those along the GS are predominant. We will therefore call $1\sigma+$ positive and $1\sigma-$ negative.

c. *Analysis*

The modeled total response is defined as the ensemble difference between a perturbation experiment and the CTL. For example, the response to the $1\sigma+$ SST anomaly in comparison to the CTL will be noted as $(1\sigma+) - \mathrm{CTL}$. The statistical significance of the response is evaluated with the confidence interval obtained by a Monte Carlo bootstrap sampling (1000 times). Unless otherwise noted, the gray dots in the figures will denote the areas of the 95% confidence level (two sided). The total response is subsequently decomposed into the linear (symmetric) and nonlinear (asymmetric) components about the sign and size of SST anomaly. Taking $1\sigma+$ and $1\sigma-$ SST anomalies as examples, a linear response (LI) and nonlinear response (NL) will be defined as

$$\mathrm{LI} = 1/2 \times [(1\sigma+) - (1\sigma-)]$$

and

$$\mathrm{NL} = 1/2 \times \{[(1\sigma+) - \mathrm{CTL}] + [(1\sigma-) - \mathrm{CTL}]\}.$$

The significance of the linear response is evaluated by testing the null hypothesis that $1\sigma+$ and $1\sigma-$ originate

TABLE 1. Description of the experiments.

Experiments	SST Amplitude	SST Sign	Lateral boundary condition	Initial condition	Ensemble size	Simulation period
CTL	Daily climatology		6-hourly climatology (1970–2009) Nov–Apr	0000 UTC 1 Nov climatology (1970–2009)	40	Nov–Apr
$9\sigma+$	9σ	+				
$9\sigma-$		−				
$3\sigma+$	3σ	+				
$3\sigma-$		−				
$1\sigma+$	1σ	+				
$1\sigma-$		−				
$(1/3)\sigma+$	$(1/3)\sigma$	+				
$(1/3)\sigma$-		−				
$(1/9)\sigma+$	$(1/9)\sigma$	+				
$(1/9)\sigma-$		−				
ENCTL	Daily climatology		6-hourly climatology 1997/98 Nov–Apr (NCEP–NCAR)	0000 UTC 1 Nov climatology (1970–2009)	40	Nov–Apr
$EN1\sigma+$	1σ	+				
$EN1\sigma-$		−				
InitENCTL	Daily climatology		6-hourly climatology 1997/98 Nov–Apr	0000 UTC 1 Nov from individual years in 1970–2009	60	Nov–Apr
$InitEN1\sigma+$	1σ	+				
$InitEN1\sigma-$		−				
InitLBCCTL	Daily climatology		6-hourly climatology from individual years in 1950–2009	0000 UTC 1 Nov from individual years in 1950–2009	60	Nov–Dec
$InitLBC1\sigma+$	1σ	+				
$InitLBC1\sigma-$		−				

from the same population. For the nonlinear response, it tests the null hypothesis that $(1\sigma+)$ − CTL and $(1\sigma-)$ − CTL are from the same population.

A novel measure of linearity versus nonlinearity is presented in this study, which is based on the distribution of the pattern correlation of time-mean response to the opposite sign of the SST anomaly [e.g., $(1\sigma+)$ − CTL and $(1\sigma-)$ − CTL] from individual ensemble member pairs. If the overall time-mean responses of the individual ensemble pairs are predominantly nonlinear (linear), then the distribution of the pattern correlations is skewed to positive (negative). Thus, the distribution of the pattern correlations from individual ensemble member pairs provides a measure of nonlinearity independent of the statistical significance in the ensemble mean response.

3. Modeled response

a. Internal variability

Though lacking air–sea coupling, SST variability other than the annual cycle, and the tropical influence, the CTL reproduces the observed level of the winter atmospheric internal variability and the storm track in the North Atlantic sector reasonably well. The top panel of Fig. 3 compares the dominant interannual variability patterns of the November–April averaged Z_{250} and SLP in NCEP-1 (1970–2009, 40 yr) and the CTL (40 members), showing the regressed Z_{250} and SLP on the principal component time series of the leading EOF. Throughout the paper, the Z_{250} response will be shaded and the SLP response superposed as contours. When the Z_{250} and SLP responses are in phase, this highlights the equivalent barotropic nature of the forced response. In NCEP-1, the tropical influence is removed by linear regression on the leading principal component time series of the Indo-Pacific tropical SST (Révelard et al. 2016), although similar leading patterns are obtained with tropical influence included (not shown). The observed leading mode of variability for the period 1970–2009 is the NAO. The large-scale pattern and the variance explained by the leading mode from the CTL resemble reasonably well those from NCEP-1. However, there is some regional discrepancy, especially over the GS front region. This difference might be related to different SST conditions between NCEP-1 (time varying but on a coarse grid) and the CTL (daily climatology but on a finer grid). The fact that the model reproduces the observed wintertime basin-scale intrinsic mode of variability is important, since the observed and modeled quasi-steady circulation response often projects onto the dominant modes of internal atmospheric variability (Peng and Robinson 2001; Deser et al. 2004, 2007; Frankignoul and Sennéchael 2007). Comparison of the EOF1 patterns across the different sensitivity simulations suggests that this pattern is still the dominant mode albeit with minor regional-scale differences (not shown).

Figures 3c,d compares the observed and modeled 850-hPa maximum Eady growth rate σ_{Bl} (Hoskins and

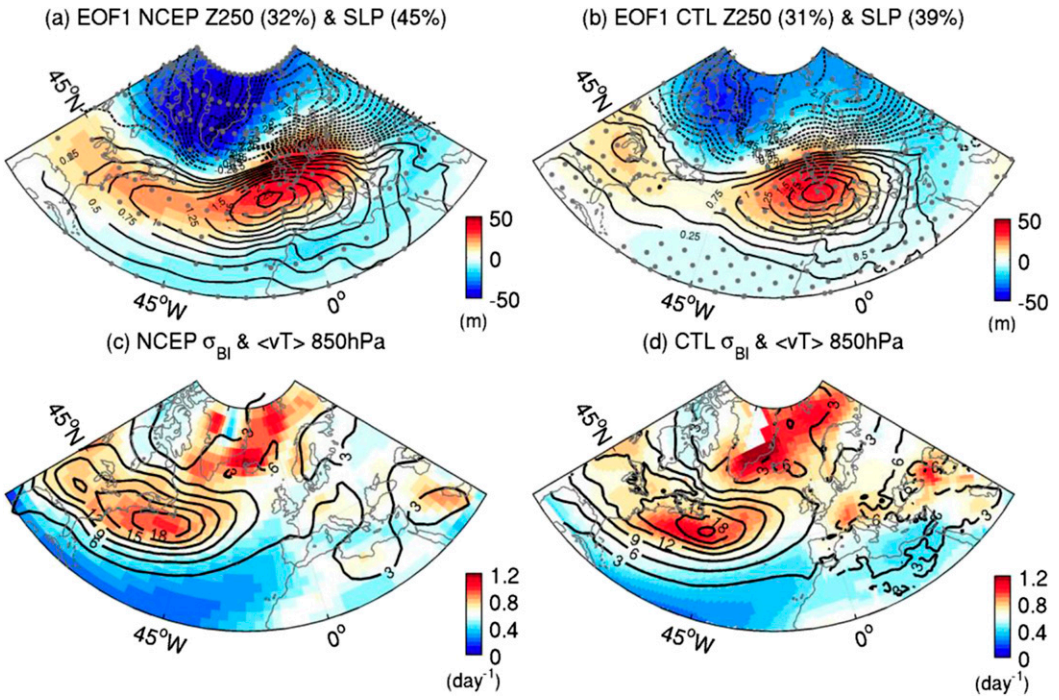

FIG. 3. (top) Comparison of domain interannual variability pattern of November–April averaged Z_{250} (color shading, m) and SLP [contours, hPa, contour interval (CI) = 0.25] from (a) NCEP-1 (40 yr, 1970–2009) and (b) CTL (40 members), showing regressions on the leading principal component time series of the November–April averaged Z_{250} and SLP. Areas of significant Z_{250} regression anomaly at the 95% confidence level are shown by gray dots. (bottom) November–April climatological mean maximum Eady growth rate $\sigma_{\rm BI}$ (color shading, day^{-1}) and the northward transient eddy heat flux $\langle|\mathbf{v}'|T'\rangle$ (contours, m s^{-1} K), both at 850 hPa, from (c) NCEP-1 and (d) CTL.

Valdes 1990), defined as $\sigma_{\rm BI} = 0.31f\,|\partial\mathbf{v}/\partial z|(1/N)$, where N is the Brunt–Väisälä frequency, f is the Coriolis parameter, and $\mathbf{v}$ is the horizontal wind vector. The figure also shows the mean northward transient (2–8-day bandpass filtered) eddy heat flux $\langle|\mathbf{v}'|T'\rangle$ at the 850-hPa level. The Eady growth rate and the transient eddy heat flux indicate the low-level baroclinicity and the storm track, respectively. Again, the CTL reproduces the observed climatology reasonably well, with the high $\sigma_{\rm BI}$ being located along the east coast of North America with the maximum over Grand Banks (Hoskins and Valdes 1990). The storm track is enhanced in the same region with the high $\sigma_{\rm BI}$, in addition to the downstream enhancement east of Greenland (Chang et al. 2002). The overall similarity between NCEP-1 and the CTL confirms that the present model is capable of representing both the internal variability and the low-level atmospheric baroclinicity during the Northern Hemisphere winter.

b. *The time-mean response*

The left two columns in Fig. 4 show the time-mean (November–April) and ensemble mean responses in Z_{250} and SLP. Focusing on the $1\sigma+$ SST anomaly case first (Fig. 4e), Z_{250} shows an anomalous ridge in the high latitudes over Greenland and two troughs in the lower latitudes, one over the GS and the other over Europe. The responses of Z_{250} and SLP are in phase; that is, the time-mean atmospheric response is equivalent to being barotropic in the vertical. Interestingly, the time-mean circulation response to the $1\sigma-$ SST forcing (Fig. 4f) is very similar to that for $1\sigma+$ SST except in relatively minor details, such as the fact that the trough in the midlatitudes is more zonally elongated from the western North Atlantic to Europe. This suggests that the quasi-stationary circulation response is nonlinear (asymmetric) about the sign of the SST anomaly. This is more clearly illustrated by breaking down the total response into the linear and nonlinear parts (Figs. 4o,p). The weak (~10 m) barotropic ridge immediately east of the GS is a linear response that appears to be consistent with the ''warm SST–ridge'' type of response discussed in past AGCM studies (Ferranti et al. 1994; Peng and Whitaker 1999; Liu and Wu 2004). The downstream ridge implies a reduced transient eddy activity and thus is consistent with Fig. 1c. Figure 4, however, also shows that the linear response (Fig. 4o) is a fraction of the total response (Figs. 4e,f). The nonlinear response (Fig. 4p) prevails with greater amplitude and spatial scale. Both

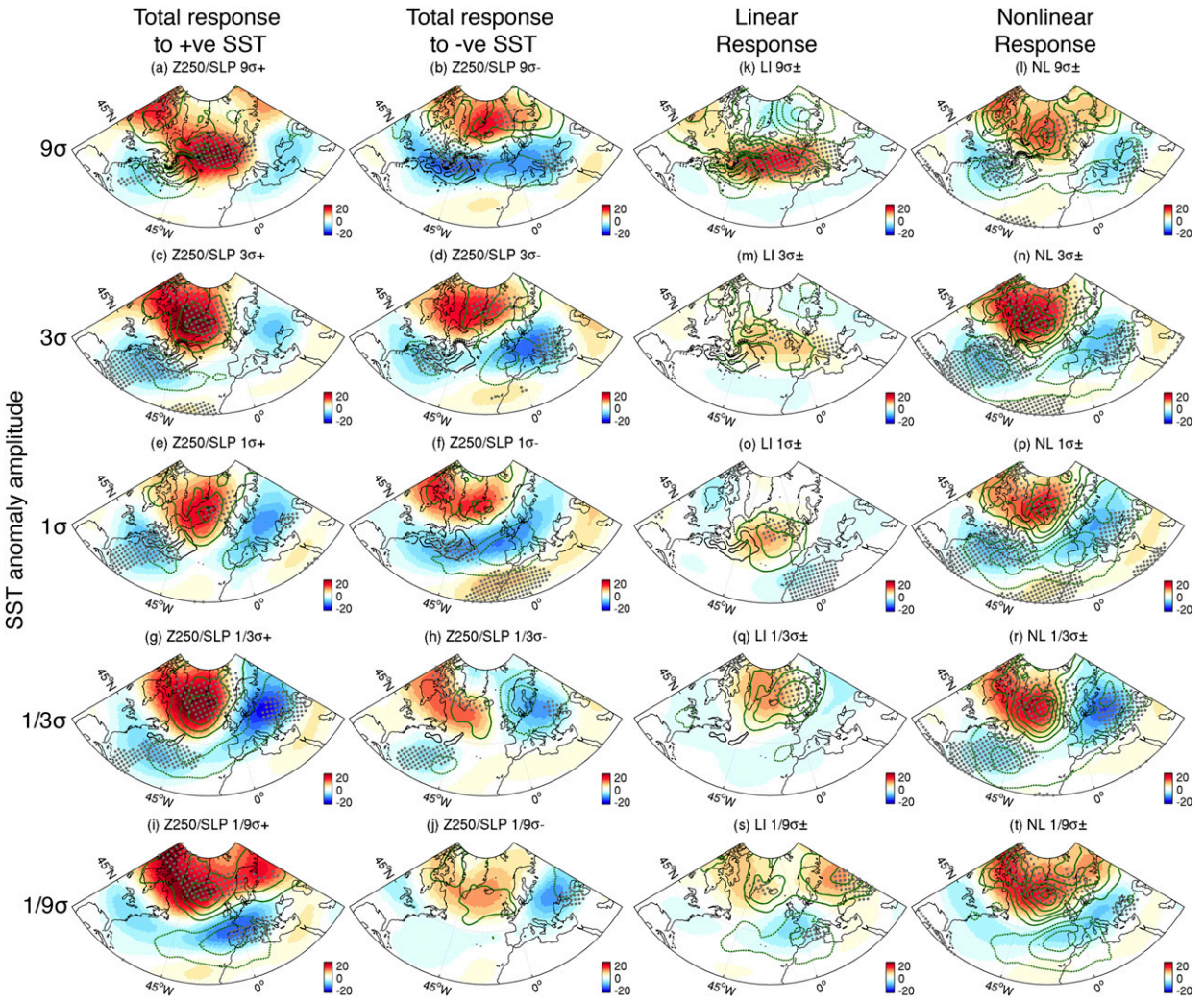

FIG. 4. The time-mean (November–April) and ensemble mean (40 members) responses in Z_{250} (shading, m) and SLP (contours, hPa, CI = 0.5 starting from ±0.5) to (a),(c),(e),(g),(i) positive and (b),(d),(f),(h),(j) negative SST anomaly patterns. Each row is for the different anomaly amplitudes decreasing from (top row) 9σ to (bottom row) $(1/9)\sigma$. Decomposition of the Z_{250} and SLP responses to the (k),(m),(o),(q),(s) LI and (l),(n),(p),(r),(t) NL parts. In (k)–(t), the SLP contour (green) interval is 0.25 starting from ±0.25. The significant response at the 95% confidence level for Z_{250} is shown by gray dots.

the nonlinear and total responses resemble the NAO, the leading wintertime mode of variability in the model (Fig. 3). The linear response pattern, in contrast, does not resemble any of the higher-order EOF patterns in the CTL (not shown), suggesting that it is a direct and forced response. Further discussion of this direct and forced response is provided in section 3e.

The nonlinear responses generated from other pairs of SST anomaly experiments with different sizes (fourth column in Fig. 4) exhibit surprisingly similar broad-scale features given that the difference in the magnitude of SST used in these experiments is up to 81 times [i.e., from $(1/9)\sigma$ to 9σ]. On the other hand, the amplitude of the linear response (third column of Fig. 4) seems to scale with that of the SST forcing (cf. Deser et al. 2004): the most prominent examples of this are the cases of $9\sigma\pm$ SST anomalies. Representing the extreme northward GS shift condition, the $9\sigma+$ SST forcing produces the equivalent barotropic ridge in the total response that is dramatically enhanced and located closer to the GS than other less dramatic SST anomalies (Fig. 4k). This is an exaggerated linear response at the expense of the comparatively weaker nonlinear response (Fig. 4l). Thus, the SST anomaly > 3°C near the GS can force the system to behave more linearly; yet, even in this case the linear response does not supersede the nonlinear response.

Figure 4 also shows that the magnitude of the time-mean total atmospheric responses is relatively insensitive

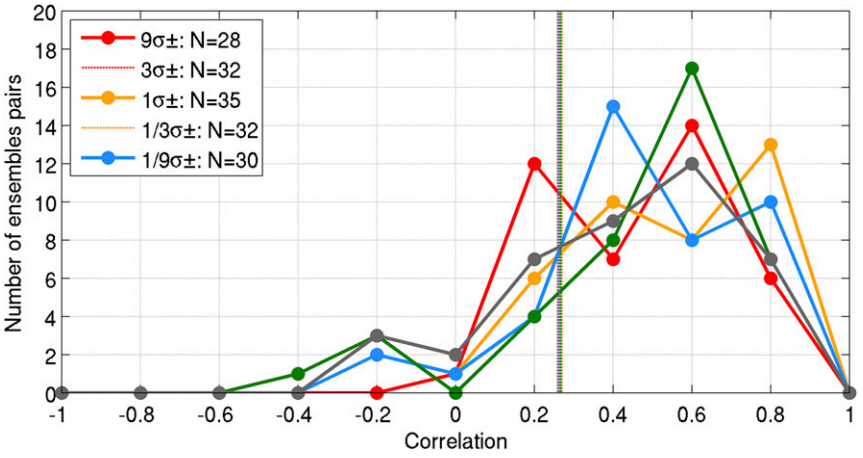

FIG. 5. Distribution of the pattern correlation of the time-mean (NDJFMA) responses to the opposite sign of the SST anomaly from each pair of the 40 ensemble members. The numbers in the legend indicate the number of ensemble pairs whose pattern correlation is significant at the 95% confidence level (closely dotted vertical lines, where the confidence level is estimated based on a Monte Carlo bootstrap sampling).

to that of the SST anomaly when the GS is shifted northward (first column). On the other hand, the magnitude of the atmospheric response tends to be more proportional to the amplitude of SST anomaly associated with the southward GS shift (second column). The nonlinearity in the amplitude of the response might be particularly more prone to taking place over the positive SST anomalies because the deeper distribution of diabatic heating (Révelard et al. 2016; also in Fig. 6) would induce more energetic circulation adjustment processes (section 3c). However, the sign of the responses remains largely unchanged regardless of the polarity of the SST anomaly patterns. Therefore, the result demonstrates the predominance of the nonlinear response over a wide range of the magnitude and sign of the SST anomaly. However, the exact location and amplitude of responses do depend on the SST anomaly.

An alternative way to demonstrate the predominant nonlinearity of the time-mean response is to compare the distribution of the pattern correlation of the response to the opposite sign of the SST anomaly from the individual ensemble pairs. Figure 5 shows the distributions of the pattern correlations over the North Atlantic (20°–80°N, 100°W–55°E), color coded to denote the five different sets of SST experiments. All five distributions of the pattern correlations are highly skewed to positive, with 67.5%–87.5% of the total ensemble pairs exhibiting statistically significant (5% level) positive correlations (dotted vertical lines). The 5% significance of the pattern correlation is estimated based on a Monte Carlo bootstrap sampling (1000 times). The high fractions of significant positive pattern correlation again suggest that the response patterns of individual member pairs are similar (i.e., nonlinear) despite the opposite sign of the SST anomaly.

c. *Vertical distribution of the response*

How are the linear and nonlinear responses distributed with height over the GS SST anomalies? Figure 6 shows the latitude–height diagrams of the response in potential temperature θ, geopotential height Z, and meridional circulation fields (v, w) averaged over the forcing region (50°–30°W) to the $1\sigma\pm$ SST anomalies. All other cases exhibit the similar behavior except in magnitude. Figures 6a, b shows that over the forcing region (35°–65°N), the total θ response reflects the sign (and amplitudes, not shown) of the SST anomaly. This is more clearly illustrated in the linear response (Fig. 6e), in which the baroclinic vertical structure of the θ response is evident. The significant positive θ anomaly of 0.2–0.3 K extends up to 300 hPa and is accompanied by the ascending motion (Czaja and Blunt 2011; Smirnov et al. 2015; Wills et al. 2016), while the significant negative θ anomaly of 0.2–0.3 K up to 600 hPa is coincident with the descending motion. The deeper extension of the diabatic heating than the cooling is consistent with the finding by Révelard et al. (2016), who attributed the uneven vertical distribution of the heating and cooling to the primary cause of the nonlinearity in observed circulation response to the changes in the Kuroshio Extension front (Qiu et al. 2014).

The nonlinear response of the meridional circulation is weak in the area where the linear circulation response

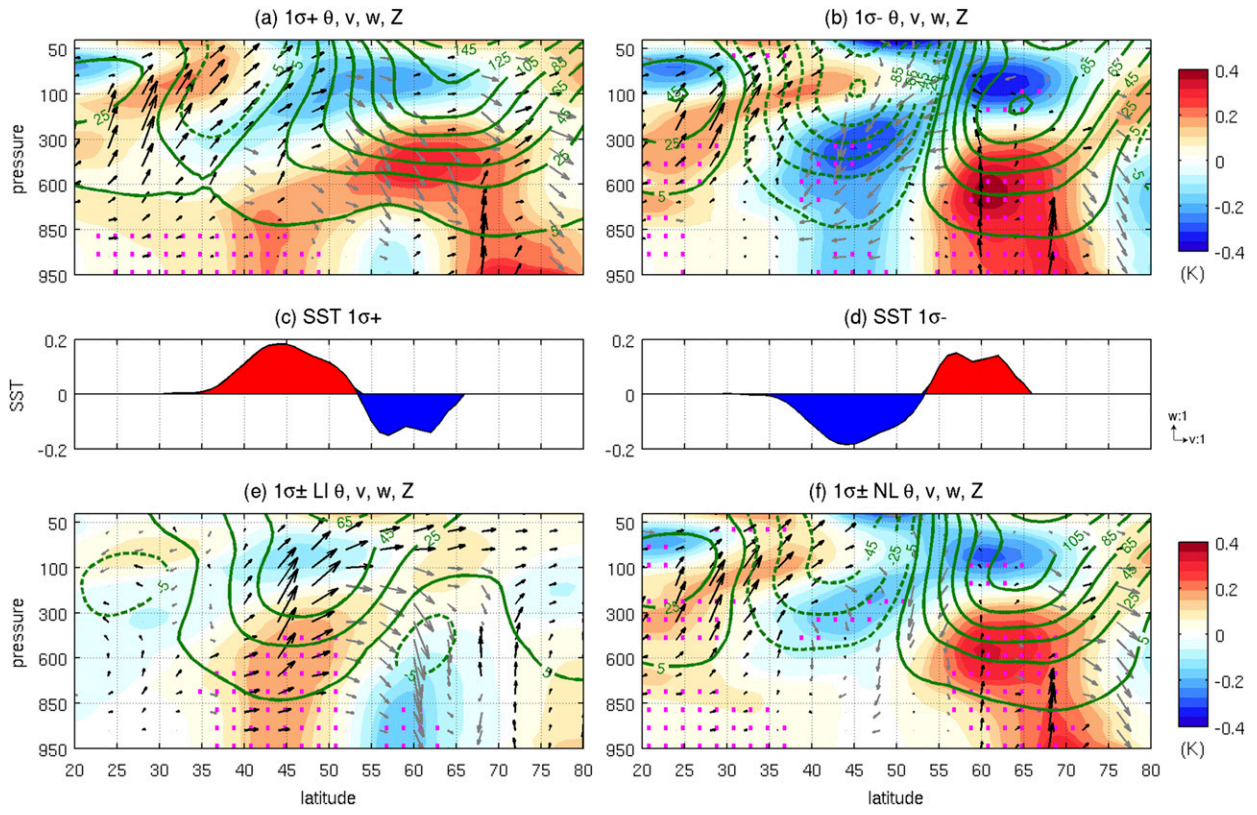

FIG. 6. (top) Latitude–height cross-sections of the total response in potential temperature θ (K, colored shading), geopotential height Z (m, green contours, CI = 20, starting from ±5) and v–w wind vectors (m s^{-1}, black arrows for upward, gray downward), averaged over the forcing region (50°–30°W) for (a) 1σ+ and (b) 1σ−. (middle) Meridional profiles of (c) 1σ+ and (d) 1σ− SST anomaly respectively, for the same zonal band. (bottom) As in (a) and (b), but for (e) LI and (f) NL responses. The vertical wind vectors are scaled by 10^3 and the reference vector is shown to the right of the middle panels. The significance of the response of θ at the 95% confidence level is marked by magenta dots.

is strong (35°–65°N). However, to the north and aloft of the forcing region (65°–75°N), a nonlinear circulation response is apparent: it shows the upward motion that is accompanied by the warming of the whole troposphere and the nonlinear ridge response exceeding 100 m. This is to be compared to the much weaker linear ridge response (~45 m) over warm/cold SSTs at 45°N. This nonlinear ridge response would block and displace the westerly jet, resulting in cyclonic wave breaking in the high-latitude North Atlantic (section 3e).

d. Emergence and evolution of the nonlinear response

How do the linear and nonlinear responses emerge over time? Figure 7 shows the biweekly development of the weekly averaged Z_{250} and SLP responses for the 1σ+ case. All other cases show similar patterns (see Fig. 8b). The response is initially (in week 1) weak and baroclinic (although not evident in the figure because of the color scale) but rapidly develops into the equivalent barotropic response in weeks 2 and 3 (Deser et al. 2007; Seo et al. 2014). By week 7, the equivalent barotropic ridge appears over Iceland and southeast of Greenland, which resembles the time-mean total response pattern. The ridge response emerges again in weeks 15–17 and 23, though during these periods the response is noticeably weaker. The time series of the Z_{250} response averaged over southeast Greenland (the box in week 1) is shown in Fig. 8a for the 1σ+ and 1σ− cases. Both responses exhibit the ridge peaks in weeks 6 and 7, which lasts 5–6 weeks. The blocking detection calculation, the detailed methodology of which is discussed in section 4b, indicates that this intraseasonal modulation of the ridge response is associated with the evolution of the anomalous blocking event. Decomposition of the total response into the linear and nonlinear responses reaffirms that the strong ridge response in this region is, for the most part, nonlinear and is related to anomalous blocking. Note that there are other periods when the total response appears to be linear, for example, weeks 14–17. However, the associated amplitude of the ridge response is too small to contribute to the time-mean ridge response significantly. It is intriguing that the Z_{250}

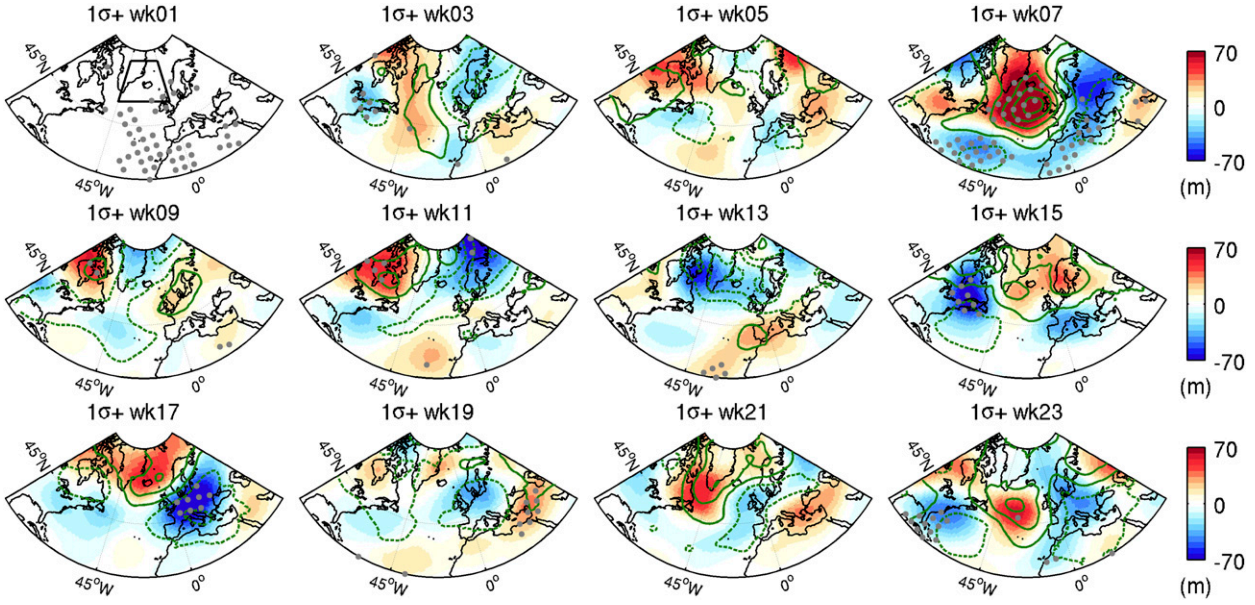

FIG. 7. Weekly averaged Z_{250} (colored shading, m) and SLP (contours, hPa, CI = 2 starting from ±1) responses for the 1σ+ SST anomaly case. Shown is the evolution of every other week starting at top left from week 1. The significance of Z_{250} anomaly at the 95% confidence level is shown by gray dots. The box in week 1 denotes the area for averaging in Fig. 8.

response evolves coherently not only when comparing 1σ+ and 1σ− (Fig. 8a) but also across the first 10 SST perturbation experiments (Fig. 8b).

e. Precipitation response

From sections 3b–d it was shown that the linear response is smaller in magnitude and baroclinic in the vertical, and confined to the vicinity of the SST forcing. This is in contrast to the nonlinear response showing an equivalent barotropic structure that is hemispheric in scale as shown in other previous studies (e.g., Deser et al. 2007). While the linear response is of small amplitude, it can be nevertheless important regionally. Figure 9 compares the linear and nonlinear responses in precipitation. The magnitude of the nonlinear response remains similar with various amplitudes of SST forcing, consistent with the notion that the level of internal variability remains largely the same across the experiments. The patterns of the nonlinear response show the increased (decreased) rainfall response in the subtropical (subpolar) North Atlantic, which resemble the equilibrium nonlinear and total Z_{250} response patterns, suggesting that the nonlinear rainfall response is indeed controlled by the dominant mode of internal variability. In contrast, the amplitude of the linear response is proportional to that of the SST forcing, with the significant responses (indicated with dots) found directly over the GS SST forcing region. This reinforces the fact that the linear response is not associated with the internally generated dominant mode of atmospheric variability in the CTL (Deser et al. 2004), but it is directly forced by the SST anomaly.

Despite the regional importance, however, within the observed range of SST anomalies, the linear response makes little contribution to the basin-scale circulation response when measured as the quasi-steady responses in Z_{250} and SLP. Only when the unrealistically large diabatic forcing is used as in the experiments 9σ±, the linear response becomes of tantamount importance to the nonlinear response. Therefore, any further discussion on the relative importance of linear versus nonlinear response might be fruitless, as the conclusion would be sensitive to the chosen amplitude of SST forcing in the experiment. The linear response of the extratropical atmosphere to the SST anomalies related to the western boundary currents has been discussed in some of the previous literature (e.g., Smirnov et al. 2015; Kuwano-Yoshida and Minobe 2017), while the nonlinear response has not been addressed in detail. The rest of the paper will therefore focus on the processes leading to the nonlinearity of the response.

f. Nonlinear rectification effect on the mean state

The fact that the response patterns are similar and that they evolve consistently independent of the size and sign of SST anomalies suggests that different SST anomalies have led to a similar quasi-steady mean state. In the North Atlantic, a salient feature of the change in the mean state may well be the displacement of the

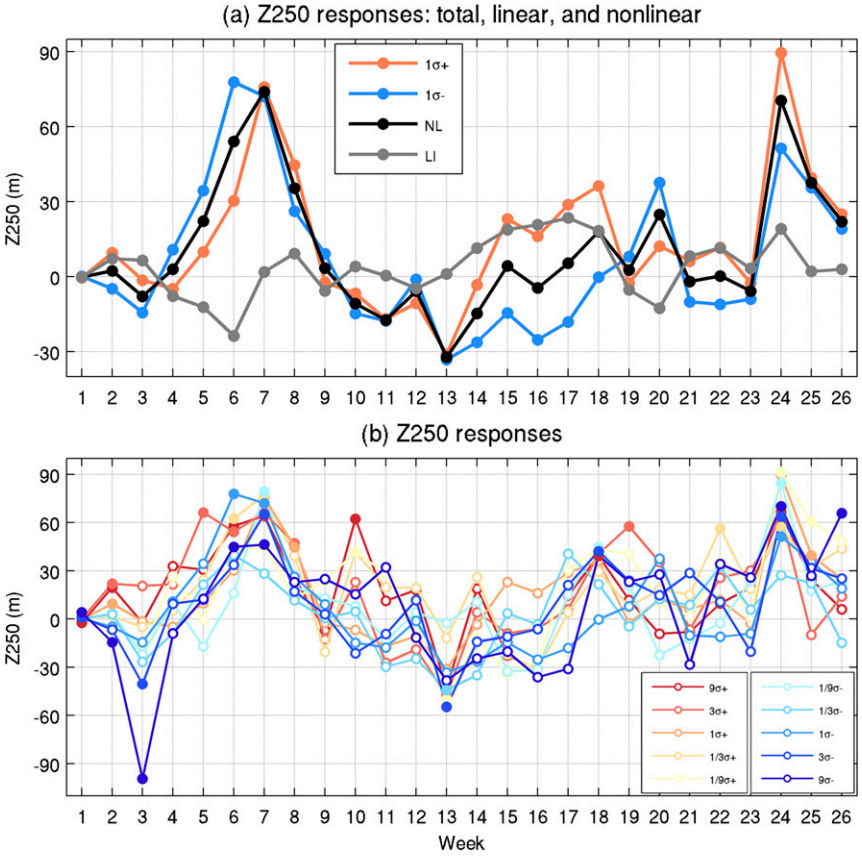

FIG. 8. Weekly evolutions of the area-averaged Z_{250} (m) over Greenland (55°–70°N, 45°W–0°E; see the box in Fig. 7). (a) The total responses for the case of $1\sigma+$ (orange) and $1\sigma-$ (blue) SST anomalies, overlaid with the LI (gray) and NL (black) responses. (b) Evolution of the total Z_{250} responses color coded to represent 10 perturbation simulations.

eddy-driven jet associated with the variations of the storm track and the atmospheric blocking (Woollings et al. 2010b). Our working hypothesis is that the ridge response near Greenland is a signature of a persistent blocking that is associated with the higher occurrence of the eddy-driven jet in its southern position and the negative NAO-like quasi-steady response.

To diagnose the shift in the eddy-driven jet, we use the jet latitude index by Woollings et al. (2010b). Figure 10a shows the histograms, with a bin size of 2.5° latitude, of the daily maximum U_{850} as a function of latitude between 20° and 80°N for the first 11 SST perturbation experiments. The daily DJF U_{850} fields are zonally averaged over the North Atlantic (60°W–0°) and then smoothed over 5 days to remove the high-frequency transients. The histogram of the daily jet latitude estimated from the 40-yr NCEP-1 DJFs (gray) shows the three characteristic peaks at the southern (37.5°N), central (45°N), and northern (57.5°N) positions. In NCEP-1, the North Atlantic jet is found to occur for 502 and 483 days out of 3600 days (i.e., 40 DJFs) in central and northern latitudes, respectively, while the southern jet position is observed for 278 days. The simulated jet latitude distribution in the CTL (black) grossly captures the three preferred latitudes of the observed eddy-driven jet position (Woollings et al. 2010b; Davini and Cagnazzo 2014), although there are apparent biases in the model, such as the overestimation of the occurrence at the central latitude, the southward displacement of the northern position, and the underestimation of the occurrences of the southern position. The histograms for both $1\sigma+$ and $1\sigma-$, marked as thick red and blue lines, respectively, as well as all other perturbation experiments (thin lines), show the increased occurrence of the southern jet position compared to the CTL. For example, the jet spends 269 (300) days in the southern position (35°N) in $1\sigma+$ ($1\sigma-$) in comparison to the 180 days in the CTL, thus representing 50% (67%) more frequent occurrences in the southern position. All other experiments show the similar increase in the days with a southerly shifted jet compared to the CTL (Fig. 10), and the Monte Carlo

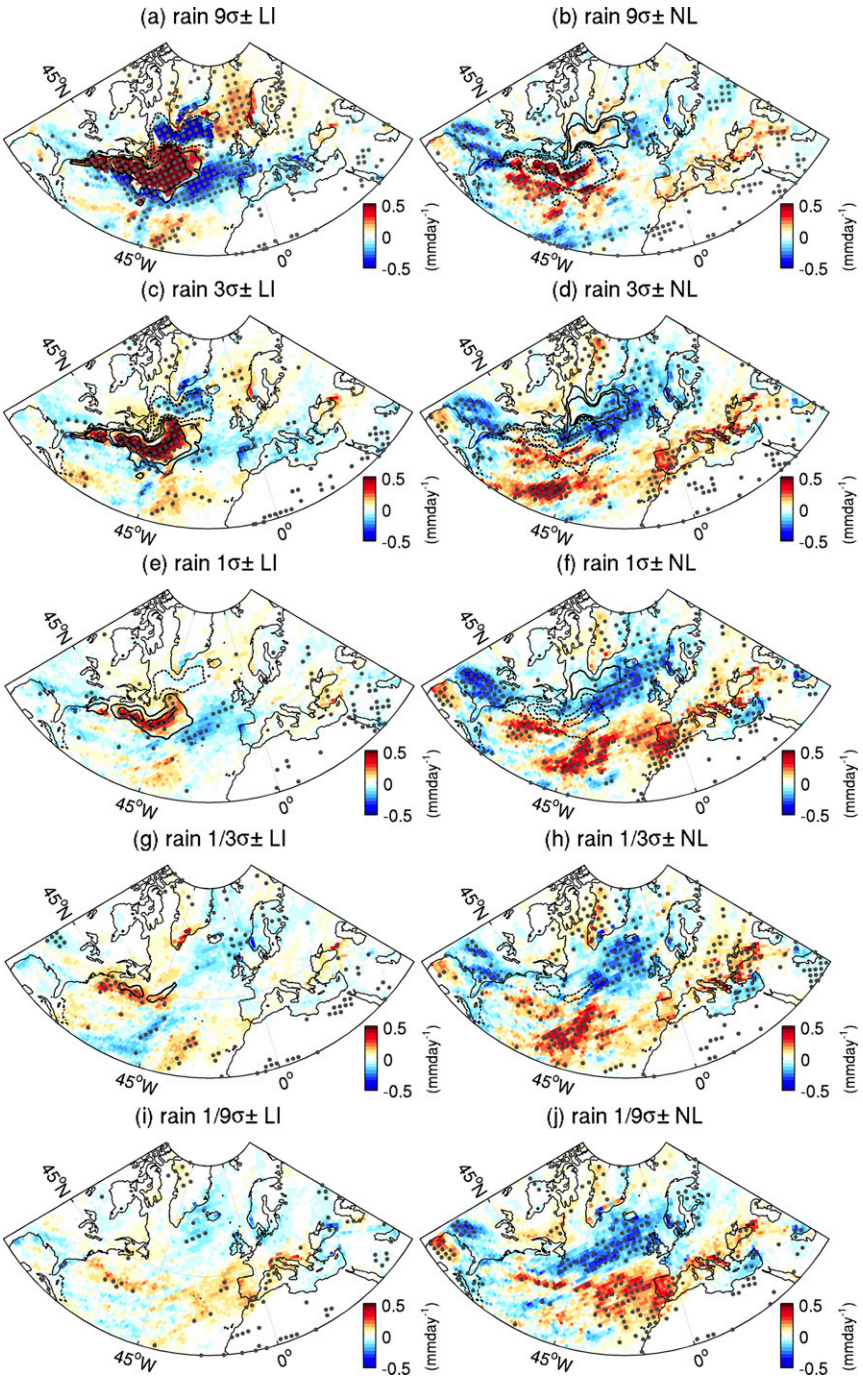

FIG. 9. (left) LI and (right) NL precipitation (mm day^{-1}) response with varied sizes of SST forcing. The significant response at the 95% confidence level is shown by gray dots.

testing of the composite mean difference of the jet occurrence at 35°N between the SST perturbation experiments and the CTL indicates that these increases are statistically significant at the 99% confidence level. The consequence of the shift in the jet is discussed in the following section.

4. Role of high- and low-frequency dynamics

To explain the atmospheric dynamical adjustment processes associated with the southward shift in the jet and the equivalent barotropic ridge in the subpolar North Atlantic, this section examines separately the

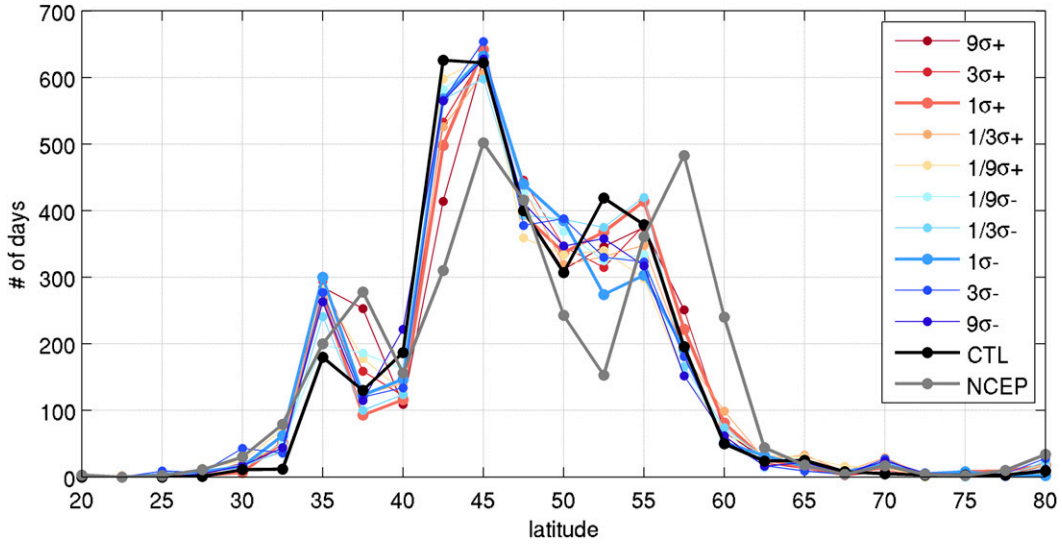

FIG. 10. Histograms (with the bin size of 2.5° latitude) of the daily jet latitude based on the zonally averaged (over the North Atlantic, 60°W–0°) and 5-day smoothed daily U_{850} from the 40 winters (DJF), color coded (see legend) to represent the 11 experiments. The jet latitude distribution from NCEP-1 is estimated from the daily U_{850} from 40 yr (1970–2009) of DJF. Results from the $1\sigma+$ and $1\sigma-$ SST anomalies, and CTL and NCEP-1 are shown as thicker lines.

high-frequency process, mainly related to the barotropic transient eddy feedback, and the low-frequency process, which is associated with the wave-breaking events in the high-latitude North Atlantic.

a. High-frequency dynamics

The change in transient eddy activity can strengthen the formation of a blocking ridge through the anomalous convergence of the eddy vorticity flux (Hoskins and Karoly 1981; Hoskins et al. 1983; Hendon and Hartmann 1982; Peng and Whitaker 1999; Seo et al. 2014; O'Reilly et al. 2016). To quantify the role of the barotropic transient eddy feedback, we focus on the upper-level flow and calculate the Z_{250} tendency solely caused by anomalous vorticity flux convergence Z_t^{HF} from a quasigeostrophic potential vorticity equation (e.g., Lau and Nath 1990),

$$\left(\frac{\partial Z_{250}}{\partial t}\right)^{\mathrm{HF}} = Z_t^{\mathrm{HF}} = \frac{f_o}{g}\nabla^{-2}[-\nabla\cdot(\overline{\mathbf{v}'\zeta'} + \overline{\overline{\mathbf{v}}\zeta'} + \overline{\mathbf{v}'\overline{\zeta}})], \qquad (1)$$

where primes denote the 8-day high-passed daily fields and the overbars the 8-day low-passed daily fields. The second and third terms in (1) are very small and therefore the right-hand side of (1) is dominated by the first term. Without the compensating baroclinic effect (Lau and Nath 1990), the barotropic eddy feedback at the upper level tends to strengthen the basic flow and hence is regarded as an upper bound on the total eddy feedback (Nakamura et al. 1997). Figure 11 shows the total responses of Z_t^{HF} to the $1\sigma+$ and $1\sigma-$ SST anomalies. In both cases, the barotropic transient eddy feedback is positive in the subpolar North Atlantic and is spatially well congruent to the anomalous ridge (solid contours). Likewise, the negative transient eddy feedback to the south of the ridge is in agreement with the anomalous troughs (dashed).

To further assess the importance of the transient eddy feedback, we calculate the composite evolution of Z_t^{HF} following the life cycle of a blocking ridge near Greenland. The Greenland blocking ridge time series is defined following Nakamura et al. (1997) as the 8-day low-pass-filtered Z_{250} at the center of the equivalent barotropic ridge (60°N, 40°W). From this slowly varying Z_{250}, the onset day of a blocking ridge is defined when the amplitude exceeds a positive one standard deviation and persists for at least five consecutive days. Then the composite anomalies of Z_t^{HF} are accumulated from 5 days before to 5 days after the onset of a ridge at the 1-day interval. The color shading in the left column of Fig. 12 shows the time-integrated Z_t^{HF} from day −4 to day +2, initialized from the composite low-passed Z_{250} anomaly at day − 5. The contours denote the 8-day low-pass-filtered Z_{250} response, which indicates the evolution of a slowly varying height anomaly in association with the life cycle of a blocking ridge. From the sequence of the composite evolutions for the $(1\sigma+)-$ CTL case, it is clear that the barotropic forcing by high-frequency transient eddies contributes to the development of the quasi-stationary Z_{250} ridge response near

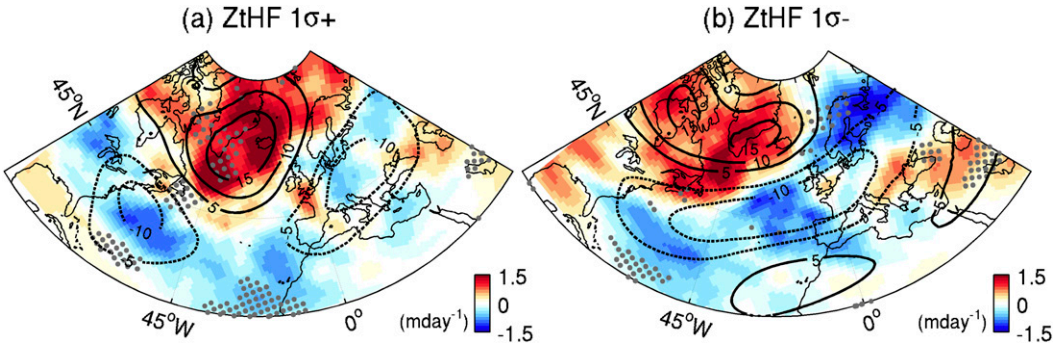

FIG. 11. The response of $(\partial Z_{250}/\partial t)^{\mathrm{HF}}$, the time rate of change of Z_{250} solely a result of high-frequency (2–8 day) transients Z_t^{HF} (m day^{-1}, colored shading), overlaid with the time-mean Z_{250} response (contours, m, positive solid, negative dashed, CI = 5). Areas of significant response at the 95% confidence level for Z_t^{HF} are shown as gray dots.

Greenland throughout the composite life cycle of a blocking ridge.

This positive feedback by high-frequency transient eddies can be compared to the evolution of the 8-day low-pass-filtered total Z_{250} tendency, $(\partial\overline{Z}_{250}/\partial t)^{\mathrm{TOT}} = Z_t^{\mathrm{TOT}}$, where the overbar indicates the 8-day low-pass filtering (Fig. 12, middle). The time integration is calculated in the same manner as the transient forcing for the corresponding lag. It is evident that the transient eddy feedback accounts for a substantial part of the low-frequency total height increase associated with the amplification of the blocking. Figure 13a summarizes its contribution by the high-frequency transients to the low-passed total Z_{250} increase, color coded to represent the first 10 SST perturbation experiments. The composite Z_t^{HF} and Z_t^{TOT} are averaged at each lag around the center of the Greenland blocking (45°–75°N, 65°–15°W). The Z_{250} increase by the transient eddy activity grows linearly over time, and at the onset of a block (day 0) the high-frequency transient eddy feedback accounts for about 50% of the low-frequency Z_{250} increase. Though the fractional contributions vary with different SST forcings, the results from all experiments point to the ubiquitous and significant role by the high-frequency transient eddy feedback in the blocking formation.

b. Low-frequency dynamics

That the transient eddy effect explains a substantial portion of the low-frequency total Z_{250} increase, but not all, indicates that the remaining fraction must be associated with processes on a longer time scale. Nakamura et al.'s (1997) composite analysis of the European blocking revealed a quasi-stationary wavy signature of Z_{250} associated with the blocking formation. In their composite analysis, the wave activity density flux emanates from upstream and converges over Scandinavia to reinforce the blocking ridge. The contours in Fig. 12, denoting the low-pass-filtered Z_{250}, also illustrate the slow evolution of Z_{250} that resembles what Nakamura et al. (1997) attributed to a quasi-stationary Rossby wave train. The wave train in the upper level extends from the eastern Pacific toward Europe when a block is formed near Greenland. Nakamura et al. (1997) inferred the role of the low-frequency dynamics in the formation and maintenance of the block by calculating the hypothetical $Z_t^{\mathrm{LF}} = Z_t^{\mathrm{TOT}} - Z_t^{\mathrm{HF}}$ at each lag, that is, the Z_{250} increase as a result of the low-frequency dynamics. The composite evolution of the time-integrated Z_t^{LF} response for the $(1\sigma+)$ − CTL case is shown in the right column of Fig. 12. It is evident that the contribution by the low-frequency dynamics to the blocking ridge is comparable to that by high-frequency feedback, particularly during the amplifying stage of a block. To substantiate that these anomalies are disturbances associated with Rossby waves, the difference in the wave activity density flux is superposed (vectors). The difference in direction and amplitude of the quasi-stationary wave train suggests that the anomalous wave activity flux emanates from the trough in the eastern Pacific and converges toward the amplifying ridge over Greenland. Figure 13c summarizes the contribution by the low-frequency fields to the total Z_{250} increase; again, although the fractions exhibit considerable spread across the experiments, it is evident that the low-frequency contribution to the blocking ridge is comparable to that by a high-frequency transient eddy, especially in the amplifying stage of a block.

How is the low-frequency process involving Greenland blocking related to the shift in the North Atlantic jet and the quasi-steady circulation response pattern? To answer this, we calculate the 2D blocking index for the North Atlantic sector. Using the daily December–February (DJF) Z_{500}, the blocking day is defined as the time and location when the reversal of the Z_{500} meridional gradient persists at least five consecutive days (Scherrer et al. 2006; Häkkinen et al. 2011). The blocking day statistics obtained this way are equivalent to

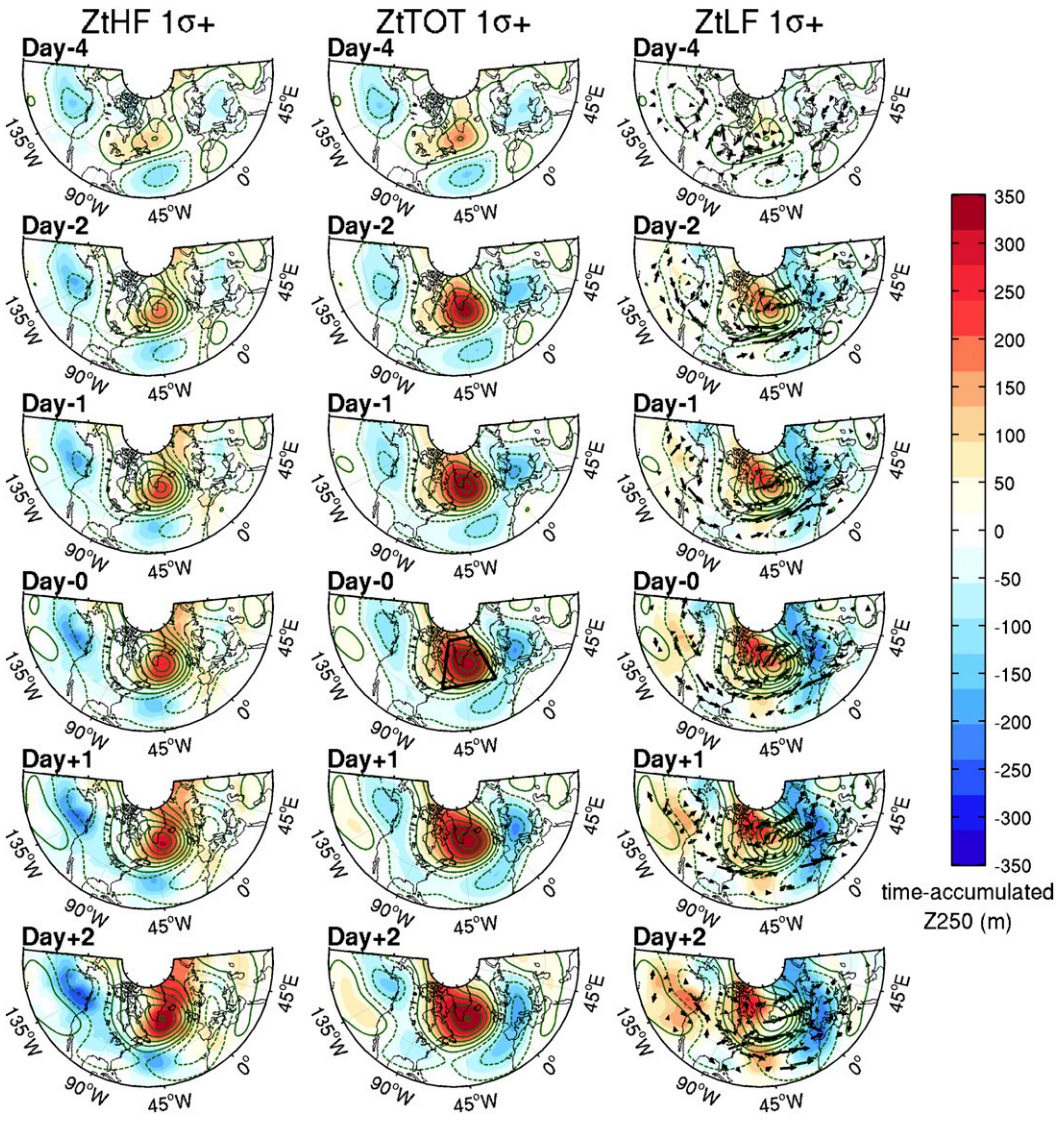

FIG. 12. Composite evolutions of the time-integrated (left) Z_{250} responses (m, colored shading) solely a result of high-frequency (2–8 day) transients Z_t^{HF}, (middle) low-pass-filtered total Z_{250} responses Z_t^{TOT}, and (right) hypothetical Z_{250} responses as a result of low-frequency process Z_t^{LF}, shown for the $1\sigma+$ SST anomaly case. The right column shows the composite evolutions of the responses in wave activity density flux (vectors). All three columns show the 8-day low-pass filtered Z_{250} (green contours). The black box at day 0 in the middle column indicates the area (45°–75°N, 65°–15°W) for averaging at each lag in Fig. 13. See text for details regarding the time integration and derivation of Z_t^{LF}.

large-scale quasi-stationary wave-breaking events (Pelly and Hoskins 2003), which over Greenland are consistent with the persistent cyclonic wave-breaking events (Davini et al. 2012). Figures 14a,b show the fractional changes of the number of blocking days (shading) in $1\sigma+$ (Fig. 14a) and $1\sigma-$ (Fig. 14b) relative to that from the CTL. Both SST perturbation experiments produce twice as many blocking days over Greenland than the CTL. This is consistent with the result above that the eddy-driven jet in both perturbation experiments occupies the southern position for 50% (67%) more days in $1\sigma+$ ($1\sigma-$) than in the CTL (Fig. 10). The corresponding composite differences in Z_{250} (contours) show the anomalous quasi-stationary ridge over Greenland in association with the enhanced occurrence of the blocking. Therefore, the higher occurrence of the high-latitude blocking in the perturbation experiments reinforces the southerly location of the eddy-driven jet and facilitates the NAO-like quasi-stationary circulation response.

In summary, the analysis reveals that both the high-frequency transient eddy feedback and the low-frequency

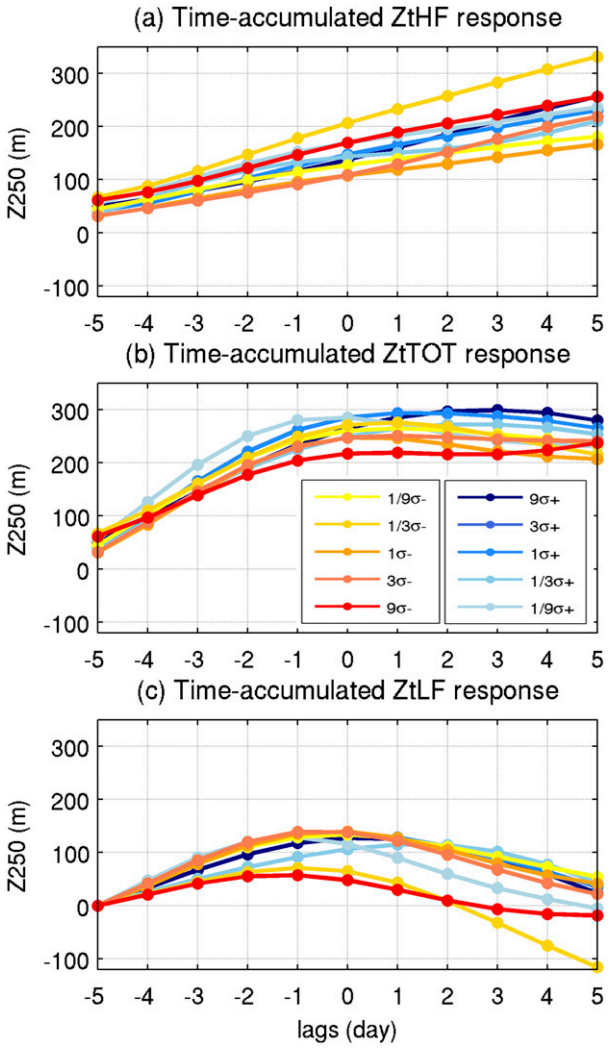

FIG. 13. Composite evolutions of the time-integrated responses of (a) Z_t^{HF} (m), (b) Z_t^{TOT} (m), and (c) Z_t^{LF} (m), area averaged at each lag over 45°–75°N, 65°–15°W (black box in Fig. 12) associated with the life cycle of the Greenland blocking from day −5 to day +5. The composite low-passed Z_{250} response at day −5 from each comparison is used as the initial conditions. The responses are color coded to represent the results from the 10 SST perturbation experiments.

wave-breaking events contribute to the equivalent barotropic ridge anomaly over Greenland. Especially important is the increased tendency for the southerly position of the eddy-driven jet, accompanied by the more frequent blocking events over Greenland, for the modeled negative NAO-like quasi-stationary responses.

5. Influence of IC and LBC

How sensitive is the nonlinearity of the response to the GS SST anomaly to the chosen initial condition (IC) and lateral boundary condition (LBC)? This issue is explored in this section through additional sensitivity experiments. First, we repeat the experiments CTL, 1σ+, and 1σ− but with the LBC switched from climatology to the 1997/98 El Niño (called ENCTL, EN1σ+, EN1σ−, respectively; see Table 1). With the strong tropical influence originating from the LBC, the patterns of the time-mean response (Figs. 15a,b) considerably differ from the runs with the climatology (Figs. 4e,f). However, the responses to the positive and negative GS SST anomalies continue to yield similar patterns in terms of sign and amplitudes, with the significant responses found in the subpolar North Atlantic. Examination of the distribution of the pattern correlations of the time-mean responses in individual member pairs supports this (Fig. 16a), showing a highly skewed distribution to the positive correlation. Out of 40 ensemble members, 29 ensemble pairs (72.5%) exhibit the significant positive correlation, while only one member has a negative correlation that is not statistically significant. This suggests that, while the large-scale pattern of the response may depend on the tropical influence, the extent to which the response remains nonlinear is independent of the tropical state.

Further sensitivity experiments are conducted to test the role of different initialization methods. These runs are identical to ENCTL, EN1σ+, and EN1σ−, except that the 1 November initial state for each of the ensemble members is sampled from 60 different years for the period 1950–2009 (called InitENCTL, InitEN1σ+, InitEN1σ−, respectively; see Table 1). This initialization method is designed to more broadly sample the phase space of the atmospheric circulation (e.g., Palmer 1993) compared to the previous sets of experiments, which are initialized with the climatological mean state perturbed with white noise. Since the initial spread is greater in these runs, the ensemble size is increased to 60. One can notice from Figs. 15c,d that the ensemble mean and the time-mean responses are hardly significant in this case. This weak statistical significance does not warrant a determination of the relative importance of the linear versus nonlinear response based on the ensemble mean response. This indicates that, when a much broader initial spread is given to the ensemble members such as in these experiments, a greater ensemble size than 60 would be desired to determine the significance of the ensemble mean response.

One can, nevertheless, demonstrate the nonlinearity of the time-mean response in the individual pairs of the ensemble members using our novel metric based on the pattern correlations (Fig. 16b). Again, the distribution is skewed to positive, with 50 out of the total 60 ensemble pairs (83%) exhibiting the significant positive

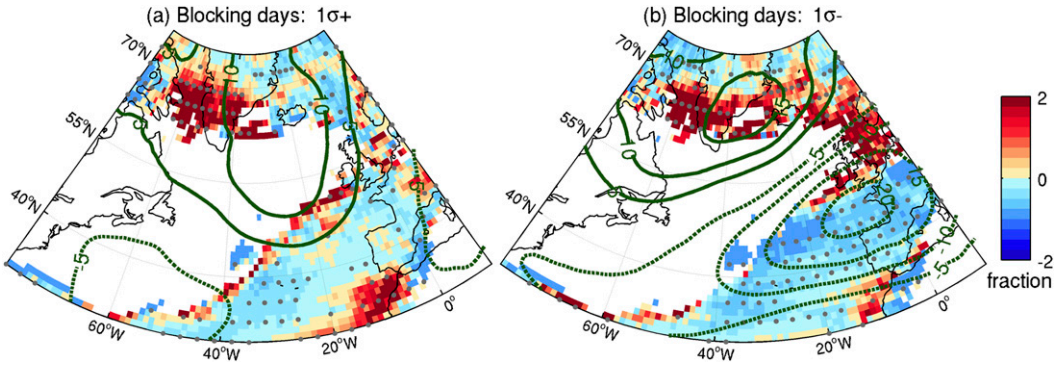

FIG. 14. Changes (colored shading, in fraction) in blocking day occurrence between (a) $1\sigma+$ SST anomaly and CTL and (b) $1\sigma-$ SST anomaly and CTL. The change is shown as $[(1\sigma+) - \mathrm{CTL}]/\mathrm{CTL}$ in (a) and $[(1\sigma-) - \mathrm{CTL}]/\mathrm{CTL}$ in (b). The difference in Z_{500} is shown as green contours (m, positive solid, negative dashed, CI = 10). The significance of the blocking day difference at the 95% confidence level is shown with gray dots and white shading is used when CTL has zero blocking days.

correlation, while only four members show a negative, statistically insignificant, correlation. This suggests that the time-mean response continues to be nonlinear to the GS SST anomaly despite the broader sampling of the phase space for the initial atmospheric field. Given the strong positive pattern correlations, it is argued that if the experiments were conducted with a much greater ensemble size, a significant nonlinear ensemble mean response should eventually emerge. This has yet to be shown, however, and will be addressed in a future study.

Both of the abovementioned two sets of experiments used the identical 1997/98 LBC for all of the ensemble members. One may ask whether this fixed LBC would

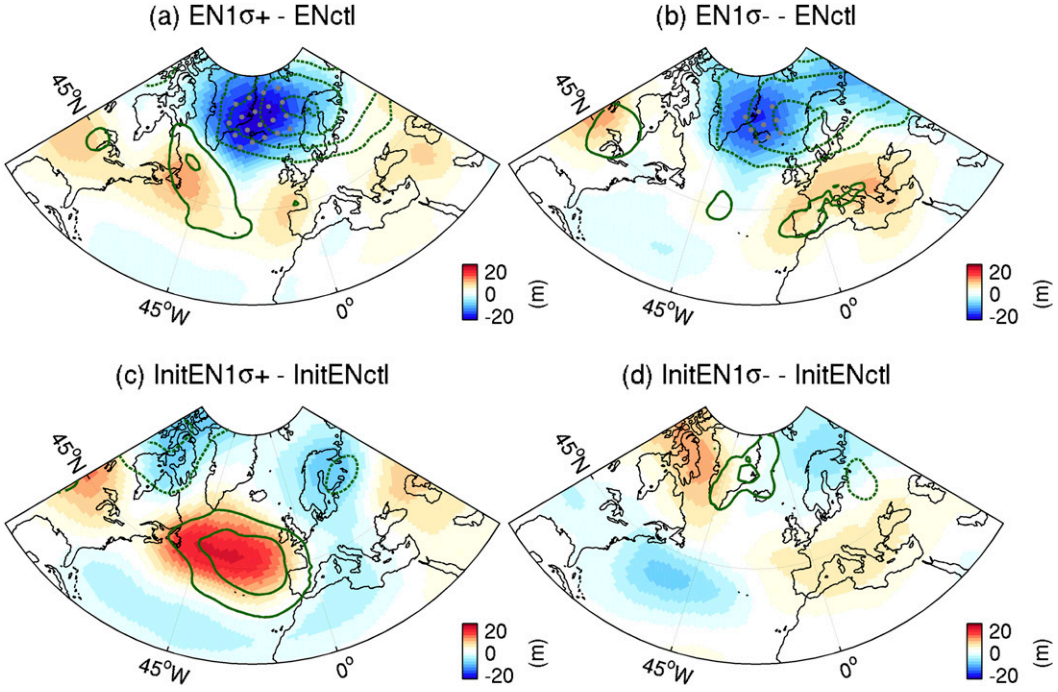

FIG. 15. The time-mean (November–April) and ensemble mean (40 members) responses in Z_{250} (colored shading, m) and SLP (contours, hPa, CI = 0.5 starting from ±0.5) to the (a) $1\sigma+$ and (b) 1σ- GS SST anomalies when the model's LBC is switched to the observed 1997/98 El Niño condition. (c),(d) As in (a) and (b), except that the ensemble IC are sampled from 1 Nov in 1950–2009 (i.e., 60 ensemble members). The significant response at the 95% confidence level for Z_{250} is shown by gray dots.

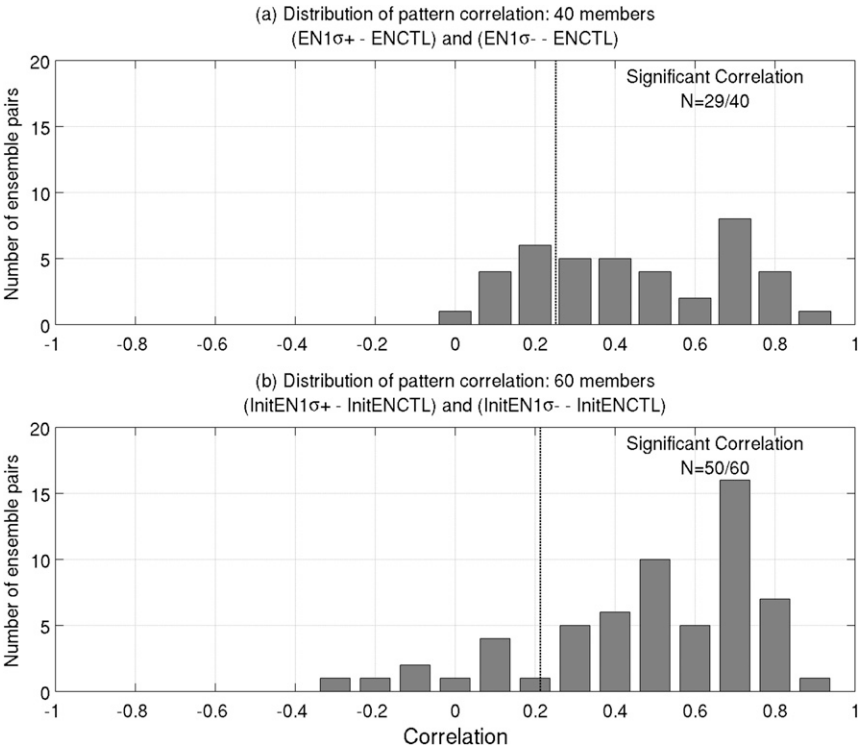

FIG. 16. Distribution of pattern correlation (a) between (EN1σ+) − ENCTL and (EN1σ−) − ENCTL using each pair of the 40 ensemble simulations, and (b) between (InitEN1σ+) − InitENCTL and (InitEN1σ−) − InitENCTL using each pair of the 60 ensemble simulations. In both panels, the distribution of correlation is skewed to positive, with 29 out of 40 (72.5%) in (a) and 50 out of 60 (83%) in (b) ensemble pairs displaying a significant (95% confidence level) positive correlation.

contribute to the nonlinearity, since all the ensemble members are influenced by the same LBCs. It should be noted that our choice of hemispheric-scale domain allows for individual ensemble members to develop a significant level of internal variability in the extratropics that is comparable to the observed one (Figs. 3a,b). To show this more explicitly, we have performed an additional set of experiments, identical to InitENCTL, InitEN1σ+, and InitEN1σ− except that the LBC in each of the ensemble members is sampled from 1 November 1950 to 31 October 2009 in the same way as the ICs are sampled. To more rigorously sample the phase space of the atmospheric circulation, the IC–LBC of mismatching years should also be considered, which is still computationally prohibitive. In this study, we limit our experiments to 60 ensemble members with the IC/LBC of the matching years repeated for each of the three SST cases. Furthermore, these experiments are from November through December only because of limited computing resources. However, note that the nonlinearity of the response is most pronounced in December (Figs. 7, 8).

Figures 17a,b compare the ensemble mean and time-mean response to the 1σ positive and negative GS SST anomalies. Overall, the two patterns are quite similar; the ensemble mean pattern correlation is 0.83. The significance of the ensemble mean response is weak, but again this is likely due to an insufficient ensemble size. Our alternative metric for nonlinearity based on pattern correlations, however, suggests that the responses in the individual ensemble pairs are highly nonlinear, with 48 pairs (80% of the total 60 ensemble pairs) showing the significant positive correlation (Fig. 17c). Only one member has a weak negative correlation, which is not statistically significant. These additional experiments confirm that the nonlinearity of the atmospheric circulation response is a robust feature found over a wide range of combinations of ICs and LBCs in addition to the sign and size of the SST anomaly.

It is also worth noting that the simulations using the 1° and ¼° NCAR Community Atmosphere Model, version 5.0 (CAM5.0), a global AGCM, forced with the time-invariant SST anomaly related to the shift in the Oyashio Extension front (Smirnov et al. 2015)—that is, experiments

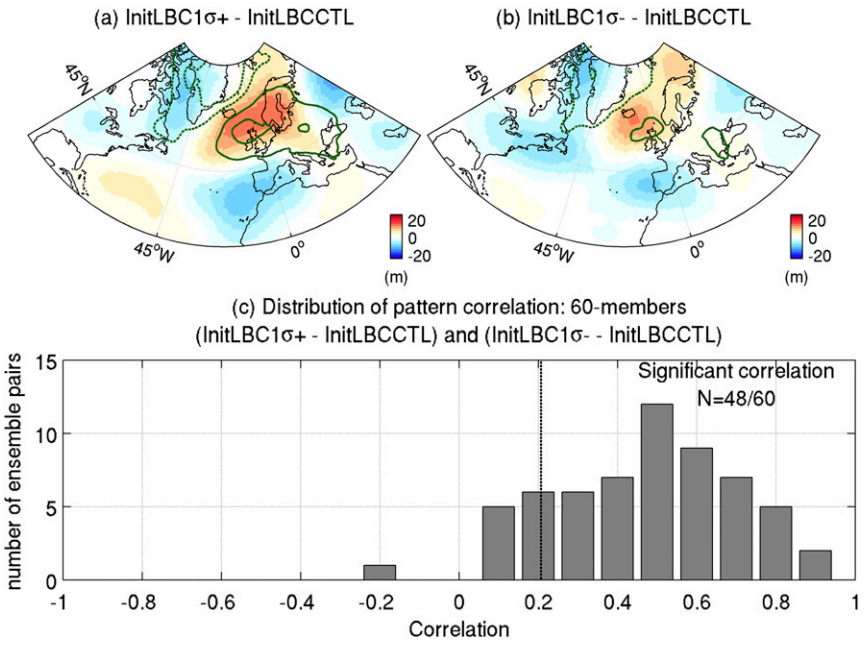

FIG. 17. The time-mean (November–December) and ensemble mean (60 members) responses in Z_{250} (colored shading, m) and SLP (contours, hPa, CI = 0.5 starting from ±0.5) to the (a) $1\sigma+$ and (b) $1\sigma-$ GS SST anomalies when the model's IC and LBC are varied between 1950 and 2009. The significant response at the 95% confidence level for Z_{250} is shown by gray dots. (c) Distribution of the pattern correlation between InitLBC1$\sigma+$ and InitLBCCTL and InitLBC1$\sigma-$ and InitLBCCTL (see Table 1 for definitions) using each pair of the 60 ensemble simulations. Again, the distribution of the correlation is skewed strongly to positive, with 48 out of the 60 total ensemble pairs (80%) displaying a significant positive correlation at the 95% confidence level.

in many aspects similar to the current study except that they use the global domain—also show a robust nonlinear response to both the positive and negative SST anomalies (Alexander et al. 2016). These CAM5 simulations were initialized from 1 November conditions of 25 different years taken from an existing CAM5 long-term hindcast simulation (Wehner et al. 2014). This, if anything, indicates that the nonlinearity would hold in the global model with a similar type of initialization scheme that more broadly samples the phase space of the atmospheric circulation.

Furthermore, Cassou et al. (2007) reported a strong nonlinear response in the model's dominant weather regimes to a reemerging tripole SST anomaly pattern in the North Atlantic using an AGCM coupled to an ocean mixed layer model. Seo et al. (2014) have reported a predominant nonlinear downstream response in the blocking ridge over the Gulf of Alaska to the SST anomaly in a marginal sea of the northwest Pacific. These independent modeling studies altogether support the assertion that some dynamical processes might exist in the Northern Hemisphere extratropical atmosphere, which generate the nonlinear forced response to the extratropical SST anomaly (Robinson 2000), especially related to the meridional shifts in the western boundary currents. Further analysis is necessary to quantify the physical processes that shape the linear and nonlinear responses to the GS SST anomalies in a global model with an enhanced ensemble size initialized from a broader phase space of the atmospheric circulation. However, this is beyond the scope of the present contribution, but it will be a subject of our future research.

6. Nonlinearity in the observed circulation response

Previous studies often compared the observational analysis based on the linear regression with the simulated responses, which can be applied only to the linear component of the responses. In contrast, the prevailing nonlinear response cannot be captured by the linear regression. The goal of this section is to attempt to find evidence for potential nonlinearity in the observed circulation through composite analysis.

We use the January–March (JFM) mean NCEP-1 Z_{250} and SLP from 1954 to 2012 to match the GSI period. The

annual cycle is removed, and the resultant time series is detrended at each grid point. The composite averages of Z_{250} and SLP are made against the detrended and normalized JFM GSI (Fig. 1a) when the GSI leads by 1 yr. This particular lag is based on the observational analysis (Kwon and Joyce 2013) showing that the significant correlation between GSI and SST exists in the winter North Atlantic when the GSI leads SST by 1 yr. This is consistent with the model experimental setup, where the atmospheric response is generated by the lagged SST anomaly associated with the GS shift 1 yr before. Because 1 yr is too long compared to the typical persistence time scale of intrinsic extratropical atmospheric variability, the 1-yr lag is interpreted to be associated with the slow evolution of SST resulting from the Gulf Stream changes, while the atmospheric anomaly should respond to the SST anomaly within a couple of weeks.

In NCEP-1, the tropical influence is removed via linear regression (Révelard et al. 2016); however, a very similar result is obtained even with the use of the full field (not shown). This suggests that the nonlinearity in the circulation response itself does not owe its existence to the tropical influence but rather to the extratropical atmospheric dynamics, a notion that is supported by the present model analysis (Figs. 15a,b). To examine the systematic behavior of the observed circulation in response to the amplitude of the GS shift, a range of GSI threshold values are considered for composite averaging using both the positive and negative thresholds for northward and southward shifts [e.g., $\pm(1/9)\sigma$, $\pm(1/3)\sigma$, $\pm1\sigma$, and $\pm(5/4)\sigma$].

Figure 18 shows that the circulation anomaly tends to be linear about the sign of the GSI when the GS deviates from the climatological position by a moderate amount [e.g., $\pm(1/9)\sigma$ and $\pm(1/3)\sigma$, which occur 86% and 75% of the time, respectively, during the 59-yr period]. The positive (negative) NAO pattern emerging 1 yr after the northward (southward) GS shift is suggestive of the influence of the GS excursions on the NAO pattern. Since the maximum positive correlation is known to exist between the NAO and GSI when the NAO leads the GSI by 12–18 months (e.g., Frankignoul et al. 2001), this composite analysis implies that the northward (southward) GS excursions reinforce the linear response of the GSI to the positive (negative) NAO. However, as the GSI excursions become larger—for example, at $\pm1.0\sigma$, which occurs 32% of the time—the atmospheric circulation ceases to be linear. At $\pm(5/4)\sigma$, which represents the extreme cases occurring only 15% of the time, the circulation pattern becomes completely nonlinear. The resulting nonlinear pattern features the anomalous trough over Greenland and the anomalous ridge in the lower latitudes and Scandinavia. The analysis implies that the observed extratropical circulation is linear with respect to the moderate excursions of the GS position, but it can be strongly nonlinear when the GS shifts far from its climatological position. The small sample sizes used in the analysis advise caution about more conclusive arguments. However, there are indications that the GS shift leads to a slight reinforcement of the NAO pattern when the atmospheric response is weak and linear. When the response is strong and nonlinear, however, the GS shift would give rise to an NAO pattern that is highly skewed.

Because of the short length of the GSI and the small sample size for composites for large GSI, it is problematic to define instances with a high GSI. Indeed, the amplitudes and patterns of the response are found to vary to some extent with the choice of composite thresholds. However, within a reasonable range of variations of the composite averages, the nonlinear circulation pattern appears to be maintained. We note that the observational analysis is not entirely consistent with the model results in that the observed circulation behaves nonlinearly only for the large GS excursions, whereas the modeled response is nonlinear across the range of GSI shifts. The model analysis is based on the atmospheric response to an SST pattern that is obtained 1 yr after the 1σ shift of the GSI. It is possible that, particularly for the large GS shifts, a different time lag might be required for the emergence of the SST pattern that has the maximum correlation with the GSI. This possibility is not taken into account in the current study.

7. Summary and discussion

This study investigates the extratropical atmospheric circulation response in the North Atlantic sector to meridional shifts in GS position. A large ensemble of WRF simulations is forced with a range of SST anomalies to account for various GS shift scenarios, with altered lateral boundary conditions (LBC) and a different initialization method to reflect the broad phase space of the atmospheric circulation. The results from a suite of experiments, supported in part by the independent analysis of a reanalysis product, reveals that, while the particular pattern of the response may vary with different IC and LBCs, the extratropical circulation response is highly nonlinear about the sign and size of the GS SST anomaly. The conclusion based on ensemble mean response is further supported by a novel correlation-based metric, showing that the majority of the individual ensemble pairs in each of the experiments have the significant positive pattern correlation of the time-mean responses.

The nature of the emergence and maintenance of the nonlinear response is examined in the SST perturbation

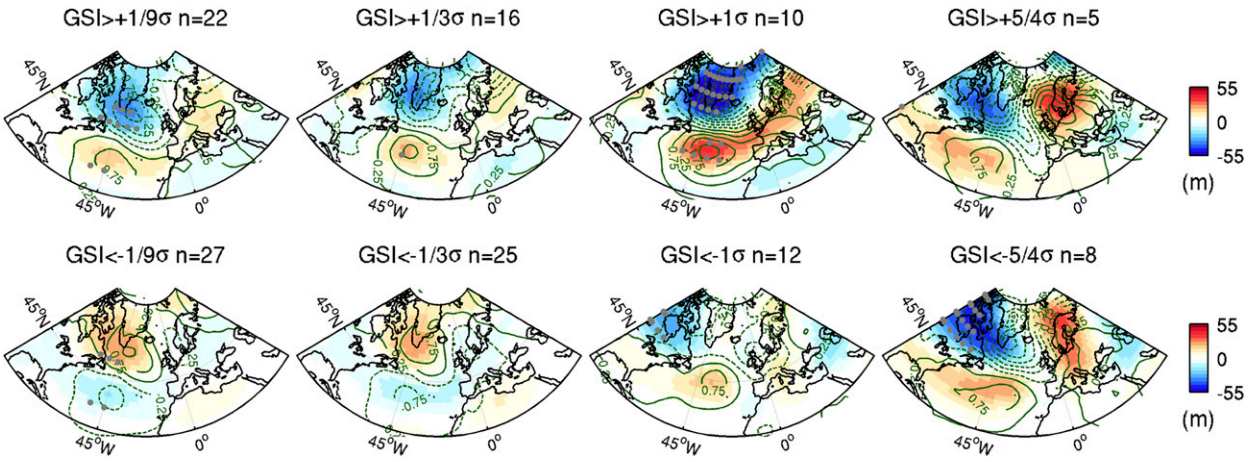

FIG. 18. Composite anomaly of the JFM Z_{250} (colored shading, m) and SLP (contours, hPa, CI = 0.5) of NCEP-1 (1959–2012) with the GSI threshold values [$(1/9)\sigma$, $(1/3)\sigma$, 1σ, and $(5/4)\sigma$] when the JFM GSI leads by 1 yr. The composite average for the (top) northward and (bottom) southward GS shift. The number of years that meets each criterion is indicated on the top of each plot. The significance of Z_{250} anomaly at the 90% confidence level is shown by gray dots.

experiments with the climatological IC and LBC. The evolution of the Z_{250} near Greenland, the center of action for the nonlinear response pattern, shows the strong ridge anomaly that is fully established by the weeks 6 and 7 in all experiments (December) and evolves over a 5–6-week period. The ridge response over Greenland is identified as the anomalous blocking events, maintained and reinforced in part by the high-frequency transient eddy feedback and in part by the low-frequency wave-breaking events. Closely related to the dynamical adjustment processes that yield the enhanced blocking over Greenland is the position of the North Atlantic eddy-driven jet. In all perturbation experiments, the jet exhibits the enhanced frequency of occurrence in the southern latitude that critically determines the model's quasi-stationary response pattern that resembles the NAO.

Additional sensitivity simulations are also carried out to explore the impact of the climatological IC and LBC on the purported nonlinearity of the response. When the climatological LBC is switched to the period of the 1997/98 extreme El Niño winter to account for the tropical influence, the spatial pattern of the equilibrium response becomes different. So, the spatial pattern of the quasi-steady response does depend on the LBC. However, the nonlinearity of the response—in terms of sign, pattern, and amplitude—is maintained. In addition to the tropical influence, the IC is chosen from 1 November of different years to more robustly sample the phase space of the atmospheric circulation. In this case, the overall statistical significance of the ensemble mean response becomes very weak as a result of an enhanced initial ensemble spread (i.e., an insufficient ensemble size). Thus, a comparison of the ensemble mean responses alone does not allow for a robust determination of the relative importance of the linearity versus nonlinearity of the response. On the other hand, the individual pairs of the responses continue to exhibit highly nonlinear responses. This is shown as the distribution of the pattern correlations of the time-mean response from the individual ensemble member pairs. Out of 60 ensemble pairs, 48 pairs display a significant positive correlation, suggesting that nonlinearity of the response clearly exists in the majority of the individual pairs.

More importantly, this result remains valid even when the LBC is switched from the fixed 1997/98 winter to the varying years, which matches the time of the ICs in each ensemble member pair. Again, the significance of the ensemble mean response remains low, but our alternative metric based on the distribution of pattern correlations reveals that the nonlinearity is clearly at play in individual ensemble member pairs, where the only difference is the sign of the GS SST anomaly. In this regard, the pattern-correlation-based metric to measure the nonlinearity of the time-mean response represents a useful diagnostic approach for AGCM studies of similar type, where the ensemble size is not always sufficient to provide a statistically significant ensemble mean response. Overall, these sensitivity experiments indicate that the nonlinearity in the circulation response to the GS SST anomaly is a robust feature found over the broad parameter space encompassing different lateral boundary and initial conditions.

We also present observational evidence that the nonlinear behavior of the extratropical atmosphere might exist in the observations, especially when the GS

exhibits a significant meridional excursion. The short data record and the small sample size for large GSI composites, however, make it difficult to grant statistical robustness to the response pattern in observations. Further analysis is necessary to dissect the relationship between the GS path and the atmospheric circulation response from high-resolution model simulations and data analysis. This is left for a future study.

Overall, the current study documents the intriguing, yet robust, behavior of the extratropical North Atlantic circulation response to the GS that is unmistakably nonlinear. It is found that this nonlinearity of the response is determined by the intrinsic midlatitude atmospheric dynamics, which in part is consistent with earlier studies that show the importance of the internal variability in determining the pattern of the forced response (Robinson 2000; Peng and Robinson 2001; Magnusdottir et al. 2004; Deser et al. 2004; Cassou et al. 2007). The extent to which the nonlinearity in the response remains to be important in the presence of other key processes or factors, such as air–sea interactions and SST variability, has yet to be investigated with a much-enhanced ensemble size.

Acknowledgments. The authors are grateful for the support from NASA (NNX13AM59G) and the NSF (AGS-1355339, OCE-1419235). The computing resources were provided by the High-Performance Computing Facility at the Woods Hole Oceanographic Institution (http://web.whoi.edu/hpc). The extensive and constructive comments from Dr. Kuwano-Yoshida and three anonymous reviewers significantly improved the manuscript. The authors also thank C. Frankignoul, M. Alexander, H. Nakamura, and Y. Ruprich-Robert for the stimulating discussions in the early stage of this research.

REFERENCES

Alexander, M., Y.-O. Kwon, C. Frankignoul, M. Newman, D. Smirnov, and J. D. Scott, 2016: The seasonality and nonlinearity of the atmospheric response to SST anomalies associated with shifts in the Oyashio Front. *Proc. 2016 Ocean Sciences Meeting*, New Orleans, LA, Amer. Geophys. Union, ASLO, and TOS, A41A-04, https://agu.confex.com/agu/os16/meetingapp.cgi/Paper/92709.

Booth, J. F., L. Thompson, J. Patoux, and K. A. Kelly, 2012: Sensitivity of midlatitude storm intensification to perturbations in the sea surface temperature near the Gulf Stream. *Mon. Wea. Rev.*, **140**, 1241–1256, doi:10.1175/MWR-D-11-00195.1.

Cassou, C., C. Deser, and M. A. Alexander, 2007: Investigating the impact of reemerging sea surface temperature anomalies on the winter atmospheric circulation over the North Atlantic. *J. Climate*, **20**, 3510–3526, doi:10.1175/JCLI4202.1.

Chang, E. K. M., S. Lee, and K. L. Swanson, 2002: Storm track dynamics. *J. Climate*, **15**, 2163–2183, doi:10.1175/1520-0442(2002)015<02163:STD>2.0.CO;2.

Chen, F., and J. Dudhia, 2001: Coupling an advanced land surface–hydrology model with the Penn State–NCAR MM5 Modeling System. Part I: Model implementation and sensitivity. *Mon. Wea. Rev.*, **129**, 569–585, doi:10.1175/1520-0493(2001)129<0569:CAALSH>2.0.CO;2.

Chou, M.-D., and M. J. Suarez, 1999: A solar radiation parameterization for atmospheric studies. Technical Report Series on Global Modeling and Data Assimilation, Vol. 15, NASA Tech. Rep. NASA/TM-1999-104606/VOL15, 38 pp.

Cione, J. J., S. Raman, and L. J. Pietrafesa, 1993: The effect of Gulf Stream–induced baroclinicity on the U.S. East Coast winter cyclones. *Mon. Wea. Rev.*, **121**, 421–430, doi:10.1175/1520-0493(1993)121<0421:TEOGSI>2.0.CO;2.

Czaja, A., and N. Blunt, 2011: A new mechanism for ocean–atmosphere coupling in midlatitudes. *Quart. J. Roy. Meteor. Soc.*, **137**, 1095–1101, doi:10.1002/qj.814.

Davini, P., and C. Cagnazzo, 2014: On the misinterpretation of the North Atlantic Oscillation in CMIP5 models. *Climate Dyn.*, **43**, 1497–1511, doi:10.1007/s00382-013-1970-y.

——, ——, R. Neale, and J. Tribbia, 2012: Coupling between Greenland blocking and the North Atlantic Oscillation pattern. *Geophys. Res. Lett.*, **39**, L14701, doi:10.1029/2012GL052315.

Deser, C., G. Magnusdottir, R. Saravanan, and A. Phillips, 2004: The effects of North Atlantic SST and sea ice anomalies on the winter circulation in CCM3. Part II: Direct and indirect components of the response. *J. Climate*, **17**, 877–889, doi:10.1175/1520-0442(2004)017<0877:TEONAS>2.0.CO;2.

——, R. A. Tomas, and S. Peng, 2007: The transient atmospheric circulation response to North Atlantic SST and sea ice anomalies. *J. Climate*, **20**, 4751–4767, doi:10.1175/JCLI4278.1.

Ferranti, L., F. Molteni, and T. N. Palmer, 1994: Impact of localized tropical and extratropical SST anomalies in ensembles of seasonal GCM integrations. *Quart. J. Roy. Meteor. Soc.*, **120**, 1613–1645, doi:10.1002/qj.49712052009.

Ferreira, D., and C. Frankignoul, 2005: The transient atmospheric response to midlatitude SST anomalies. *J. Climate*, **18**, 1049–1067, doi:10.1175/JCLI-3313.1.

——, and ——, 2008: Transient atmospheric response to interactive SST anomalies. *J. Climate*, **21**, 576–583, doi:10.1175/2007JCLI1704.1.

Frankignoul, C., and N. Sennéchael, 2007: Observed influence of North Pacific SST anomalies on the atmospheric circulation. *J. Climate*, **20**, 592–606, doi:10.1175/JCLI4021.1.

——, G. de Coëtlogon, T. M. Joyce, and S. Dong, 2001: Gulf Stream variability and ocean–atmosphere interactions. *J. Phys. Oceanogr.*, **31**, 3516–3529, doi:10.1175/1520-0485(2002)031<3516:GSVAOA>2.0.CO;2.

Gangopadhyay, A., P. Cornillon, and R. D. Watts, 1992: A test of the Parsons–Veronis hypothesis on the separation of the Gulf Stream. *J. Phys. Oceanogr.*, **22**, 1286–1301, doi:10.1175/1520-0485(1992)022<1286:ATOTPH>2.0.CO;2.

Haines, K., and J. Marshall, 1987: Eddy-forced coherent structures as a prototype of atmospheric blocking. *Quart. J. Roy. Meteor. Soc.*, **113**, 681–709, doi:10.1002/qj.49711347613.

Häkkinen, S., P. B. Rhines, and D. L. Worthen, 2011: Atmospheric blocking and Atlantic multidecadal ocean variability. *Science*, **334**, 655–659, doi:10.1126/science.1205683.

Hendon, H. H., and D. L. Hartmann, 1982: Stationary waves on a sphere—Sensitivity to thermal feedback. *J. Atmos. Sci.*, **39**, 1906–1920, doi:10.1175/1520-0469(1982)039<1906:SWOASS>2.0.CO;2.

Hong, S.-Y., J. Dudhia, and S.-H. Chen, 2004: A revised approach to ice microphysical processes for the bulk parameterization of

clouds and precipitation. *Mon. Wea. Rev.*, **132**, 103–120, doi:10.1175/1520-0493(2004)132<0103:ARATIM>2.0.CO;2.

——, Y. Noh, and J. Dudhia, 2006: A new vertical diffusion package with an explicit treatment of entrainment processes. *Mon. Wea. Rev.*, **134**, 2318–2341, doi:10.1175/MWR3199.1.

Hoskins, B. J., and D. J. Karoly, 1981: The steady linear response of a spherical atmosphere to thermal and orographic forcing. *J. Atmos. Sci.*, **38**, 1179–1196, doi:10.1175/1520-0469(1981)038<1179:TSLROA>2.0.CO;2.

——, and P. J. Valdes, 1990: On the existence of storm-tracks. *J. Atmos. Sci.*, **47**, 1854–1864, doi:10.1175/1520-0469(1990)047<1854:OTEOST>2.0.CO;2.

——, I. N. James, and G. H. White, 1983: The shape, propagation, and mean-flow interaction of large-scale weather systems. *J. Atmos. Sci.*, **40**, 1595–1612, doi:10.1175/1520-0469(1983)040<1595:TSPAMF>2.0.CO;2.

Joyce, T. M., C. Deser, and M. A. Spall, 2000: The relation between decadal variability of subtropical mode water and the North Atlantic Oscillation. *J. Climate*, **13**, 2550–2569, doi:10.1175/1520-0442(2000)013<2550:TRBDVO>2.0.CO;2.

Kain, J. S., 2004: The Kain–Fritsch convective parameterization: An update. *J. Appl. Meteor.*, **43**, 170–181, doi:10.1175/1520-0450(2004)043<0170:TKCPAU>2.0.CO;2.

Kalnay, E., and Coauthors, 1996: The NCEP/NCAR 40-Year Reanalysis Project. *Bull. Amer. Meteor. Soc.*, **77**, 437–471, doi:10.1175/1520-0477(1996)077<0437:TNYRP>2.0.CO;2.

Kelly, K. A., S. Singh, and R. X. Huang, 1999: Seasonal variations of sea surface height in the Gulf Stream region. *J. Phys. Oceanogr.*, **29**, 313–327, doi:10.1175/1520-0485(1999)029<0313:SVOSSH>2.0.CO;2.

——, R. J. Small, R. M. Samelson, B. Qiu, T. M. Joyce, M. Cronin, and Y.-O. Kwon, 2010: Western boundary currents and frontal air–sea interaction: Gulf Stream and Kuroshio Extension. *J. Climate*, **23**, 5644–5667, doi:10.1175/2010JCLI3346.1.

Kushnir, Y., and N. C. Lau, 1992: The general circulation model response to a North Pacific SST anomaly: Dependence on time scale and pattern polarity. *J. Climate*, **5**, 271–283, doi:10.1175/1520-0442(1992)005<0271:TGCMRT>2.0.CO;2.

——, W. A. Robinson, I. Blade, N. M. J. Hall, S. Peng, and R. Sutton, 2002: Atmospheric GCM response to extratropical SST anomalies: Synthesis and evaluation. *J. Climate*, **15**, 2233–2256, doi:10.1175/1520-0442(2002)015<2233:AGRTES>2.0.CO;2.

Kuwano-Yoshida, A., and S. Minobe, 2017: Storm-track response to SST fronts in the northwestern Pacific region in an AGCM. *J. Climate*, **30**, 1081–1102, doi:10.1175/JCLI-D-16-0331.1.

——, ——, and S.-P. Xie, 2010: Precipitation response to the Gulf Stream in an atmospheric GCM. *J. Climate*, **23**, 3676–3698, doi:10.1175/2010JCLI3261.1.

Kwon, Y.-O., and T. M. Joyce, 2013: Northern Hemisphere winter atmospheric transient eddy heat fluxes and the Gulf Stream and Kuroshio–Oyashio Extension variability. *J. Climate*, **26**, 9839–9859, doi:10.1175/JCLI-D-12-00647.1.

——, M. A. Alexander, N. A. Bond, C. Frankignoul, H. Nakamura, B. Qiu, and L. A. Thompson, 2010: Role of the Gulf Stream and Kuroshio–Oyashio systems in large-scale atmosphere–ocean interaction: A review. *J. Climate*, **23**, 3249–3281, doi:10.1175/2010JCLI3343.1.

Lau, N.-C., and M. J. Nath, 1990: A general circulation model study of the atmospheric response to extratropical SST anomalies observed in 1950–79. *J. Climate*, **3**, 965–989, doi:10.1175/1520-0442(1990)003<0965:AGCMSO>2.0.CO;2.

Li, Z. X., and S. Conil, 2003: Transient response of an atmospheric GCM to North Atlantic SST anomalies. *J. Climate*, **16**, 3993–3998, doi:10.1175/1520-0442(2003)016<3993:TROAAG>2.0.CO;2.

Liu, Z., and L. Wu, 2004: Atmospheric response to North Pacific SST: The role of ocean–atmosphere coupling. *J. Climate*, **17**, 1859–1882, doi:10.1175/1520-0442(2004)017<1859:ARTNPS>2.0.CO;2.

Magnusdottir, G., C. Deser, and R. Saravanan, 2004: The effects of North Atlantic SST and sea ice anomalies on the winter circulation in CCM3. Part I: Main features and storm track characteristics of the response. *J. Climate*, **17**, 857–876, doi:10.1175/1520-0442(2004)017<0857:TEONAS>2.0.CO;2.

Minobe, S., A. Kuwano-Yoshida, N. Komori, S.-P. Xie, and R. J. Small, 2008: Influence of the Gulf Stream on the troposphere. *Nature*, **452**, 206–209, doi:10.1038/nature06690.

Mlawer, E. J., S. J. Taubman, P. D. Brown, M. J. Iacono, and S. A. Clough, 1997: Radiative transfer for inhomogeneous atmosphere: RRTM, a validated correlated-k model for the longwave. *J. Geophys. Res.*, **102**, 16 663–16 682, doi:10.1029/97JD00237.

Nakamura, H., and J. M. Wallace, 1990: Observed changes in baroclinic wave activity during the life cycles of low-frequency circulation anomalies. *J. Atmos. Sci.*, **47**, 1100–1116, doi:10.1175/1520-0469(1990)047<1100:OCIBWA>2.0.CO;2.

——, M. Nakamura, and J. L. Anderson, 1997: The role of high- and low-frequency dynamics and blocking formation. *Mon. Wea. Rev.*, **125**, 2074–2093, doi:10.1175/1520-0493(1997)125<2074:TROHAL>2.0.CO;2.

O'Reilly, C. H., S. Minobe, and A. Kuwano-Yoshida, 2016: The influence of the Gulf Stream on wintertime European blocking. *Climate Dyn.*, **47**, 1545–1567, doi:10.1007/s00382-015-2919-0.

——, ——, ——, and T. Woollings, 2017: The Gulf Stream influence on wintertime North Atlantic jet variability. *Quart. J. Roy. Meteor. Soc.*, **143**, 173–183, doi:10.1002/qj.2907.

Palmer, T. N., 1993: Extended-range atmospheric prediction and the Lorenz model. *Bull. Amer. Meteor. Soc.*, **74**, 49–65, doi:10.1175/1520-0477(1993)074<0049:ERAPAT>2.0.CO;2.

——, and Z. Sun, 1985: A modelling and observational study of the relationship between sea surface temperature in the north-west Atlantic and the atmospheric general circulation. *Quart. J. Roy. Meteor. Soc.*, **111**, 947–975, doi:10.1002/qj.49711147003.

Peings, Y., and G. Magnusdottir, 2014: Response of the wintertime Northern Hemisphere atmospheric circulation to current and projected Arctic sea ice decline: A numerical study with CAM5. *J. Climate*, **27**, 244–264, doi:10.1175/JCLI-D-13-00272.1.

Pelly, J. L., and B. J. Hoskins, 2003: A new perspective on blocking. *J. Atmos. Sci.*, **60**, 743–755, doi:10.1175/1520-0469(2003)060<0743:ANPOB>2.0.CO;2.

Peng, S., and J. S. Whitaker, 1999: Mechanisms determining the atmospheric response to midlatitude SST anomalies. *J. Climate*, **12**, 1393–1408, doi:10.1175/1520-0442(1999)012<1393:MDTART>2.0.CO;2.

——, and W. A. Robinson, 2001: Relationships between atmospheric internal variability and the responses to an extratropical SST anomaly. *J. Climate*, **14**, 2943–2959, doi:10.1175/1520-0442(2001)014<2943:RBAIVA>2.0.CO;2.

——, A. Mysak, H. Ritchie, J. Derome, and B. Dugas, 1995: The difference between early and middle winter atmospheric response to sea surface temperature anomalies in the northwest Atlantic.

J. Climate, **8**, 137–157, doi:10.1175/1520-0442(1995)008<0137:TDBEAM>2.0.CO;2.

Piazza, M., L. Terray, J. Boé, E. Maisonnave, and E. Sanchez-Gomez, 2016: Influence of small-scale North Atlantic sea surface temperature patterns on the marine boundary layer and free troposphere: A study using the atmospheric ARPEGE model. *Climate Dyn.*, **46**, 1699–1717, doi:10.1007/s00382-015-2669-z.

Qiu, B., S. Chen, N. Schneider, and B. Taguchi, 2014: A coupled decadal prediction of the dynamic state of the Kuroshio Extension system. *J. Climate*, **27**, 1751–1764, doi:10.1175/JCLI-D-13-00318.1.

Révelard, A., C. Frankignoul, N. Sennéchael, Y.-O. Kwon, and B. Qiu, 2016: Influence of the decadal variability of the Kuroshio Extension on the atmospheric circulation in the cold season. *J. Climate*, **29**, 2123–2144, doi:10.1175/JCLI-D-15-0511.1.

Reynolds, R. W., T. M. Smith, C. Liu, D. B. Chelton, K. S. Casey, and M. G. Schlax, 2007: Daily high-resolution-blended analyses for sea surface temperature. *J. Climate*, **20**, 5473–5496, doi:10.1175/2007JCLI1824.1.

Rivière, G., and I. Orlanski, 2007: Characteristics of the Atlantic storm-track eddy activity and its relation with the North Atlantic Oscillation. *J. Atmos. Sci.*, **64**, 241–266, doi:10.1175/JAS3850.1.

Robinson, W., 2000: Review of WETS—The Workshop on Extra-Tropical SST anomalies. *Bull. Amer. Meteor. Soc.*, **81**, 567–577, doi:10.1175/1520-0477(2000)081<0567:ROWTWO>2.3.CO;2.

Rossby, T., and E. Gottlieb, 1998: The *Oleander* project: Monitoring the variability of the Gulf Stream and adjacent waters between New Jersey and Bermuda. *Bull. Amer. Meteor. Soc.*, **79**, 5–18, doi:10.1175/1520-0477(1998)079<0005:TOPMTV>2.0.CO;2.

Sanchez-Franks, A., S. Hameed, and R. E. Wilson, 2016: The Icelandic low as a predictor of the Gulf Stream north wall position. *J. Phys. Oceanogr.*, **46**, 817–826, doi:10.1175/JPO-D-14-0244.1.

Scherrer, S., M. Croci-Maspoli, C. Schwierz, and C. Appenzeller, 2006: Two-dimensional indices of atmospheric blocking and their statistical relationship with winter climate patterns in the Euro-Atlantic region. *Int. J. Climatol.*, **26**, 233–249, doi:10.1002/joc.1250.

Seo, H., Y.-O. Kwon, and J.-J. Park, 2014: On the effect of the East/Japan Sea SST variability on the North Pacific atmospheric circulation in a regional climate model. *J. Geophys. Res. Atmos.*, **119**, 418–444, doi:10.1002/2013JD020523.

Shutts, G. J., 1983: The propagation of eddies in diffluent jetstreams: Eddy vorticity forcing of "blocking" flow fields. *Quart. J. Roy. Meteor. Soc.*, **109**, 737–761, doi:10.1002/qj.49710946204.

Skamarock, W. C., and Coauthors, 2008: A description of the Advanced Research WRF version 3. NCAR/TN-475+STR, 113 pp., doi:10.5065/D68S4MVH.

Small, R. J., R. A. Tomas, and F. O. Bryan, 2014: Storm track response to ocean fronts in a global high-resolution climate model. *Climate Dyn.*, **43**, 805–828, doi:10.1007/s00382-013-1980-9.

Smirnov, D., M. Newman, M. A. Alexander, Y.-O. Kwon, and C. Frankignoul, 2015: Investigating the local atmospheric response to a realistic shift in the Oyashio sea surface temperature front. *J. Climate*, **28**, 1126–1147, doi:10.1175/JCLI-D-14-00285.1.

Strong, C., and G. Magnusdottir, 2008: Tropospheric Rossby wave breaking and the NAO/NAM. *J. Atmos. Sci.*, **65**, 2861–2876, doi:10.1175/2008JAS2632.1.

Taylor, A. H., and J. A. Stephens, 1998: The North Atlantic Oscillation and the latitude of the Gulf Stream. *Tellus*, **50A**, 134–142, doi:10.3402/tellusa.v50i1.14517.

Wehner, M. F., and Coauthors, 2014: The effect of horizontal resolution on simulation quality in the Community Atmospheric Model, CAM5.1. *J. Adv. Model. Earth Syst.*, **6**, 980–997, doi:10.1002/2013MS000276.

Wills, S. M., D. W. J. Thompson, and L. M. Ciasto, 2016: On the observed relationships between variability in Gulf Stream sea surface temperatures and the atmospheric circulation over the North Atlantic. *J. Climate*, **29**, 3719–3730, doi:10.1175/JCLI-D-15-0820.1.

Woollings, T., B. Hoskins, M. Blackburn, D. Hassell, and K. Hodges, 2010a: Storm track sensitivity to sea surface temperature resolution in a regional atmosphere model. *Climate Dyn.*, **35**, 341–353, doi:10.1007/s00382-009-0554-3.

——, A. Hannachi, and B. Hoskins, 2010b: Variability of the North Atlantic eddy-driven jet stream. *Quart. J. Roy. Meteor. Soc.*, **136**, 856–868, doi:10.1002/qj.625.